FACULTY OF ENGINEERING AND THE BUILT ENVIRONMENT

DEPARTMENT OF CIVIL ENGINEERING

THERMO-CHEMO-MECHANICAL MODELLING OF HYDROPOWER STRUCTURES AFFECTED BY ALKALI SILICA REACTION

Prepared by: **Bukhosi R. Nyoni**

Date: **19/02/2018**

Supervisor: **Prof. P. Moyo**

THIS RESEARCH PROPOSAL HAS BEEN SUBMITTED TO THE DEPARTMENT OF CIVIL ENGINEERING, FACULTY OF ENGINEERING AND THE BUILT ENVIRONMENT, UNIVERSITY OF CAPE TOWN, IN PARTIAL FULFILMENT OF THE REQUIREMENTS FOR A MASTER OF SCIENCE DEGREE IN CIVIL ENGINEERING.

 MSc (Eng) Civil Engineering

UNIVERSITY OF CAPE TOWN
IYUNIVESITHI YASEKAPA • UNIVERSITEIT VAN KAAPSTAD

PLAGIARISM DECLARATION

THESIS SUPERVISOR: PROF. P. MOYO

1. I know the meaning of plagiarism and declare that all the work in the document, save for that which is properly acknowledged, is my own.

2. I have used the Harvard Convention for citation and referencing. Each significant contribution to and quotation in this research from the work or works of other people has been attributed, and has been cited and referenced.

3. This thesis has been submitted to the Turnitin module and I confirm that my supervisor has seen my report and any concerns revealed by such have been resolved with my supervisor.

Name: **Bukhosi Raphael Nyoni** Student No.: **NYNBUK001**

Date: **19/02/2018** Signature: Signed by candidate

DEDICATION

To my mother, father and brother

ABSTRACT

Alkali-Silica Reaction (ASR) is a deleterious chemical reaction whose product expands in the presence of water inducing internal pressures within the concrete microstructure resulting in cracking and a reduction in elastic properties of concrete. Thus, ASR can substantially reduce serviceability and compromise the safety of concrete structures. To ensure the safe operation of these ageing structures, a sound understanding of the material deterioration and effect of ASR on the structural performance of these structures has to be developed. To this end, a number of numerical constitutive models have been developed to simulate ASR induced expansion in concrete. These models can generally be categorised as either, (i) microstructural models which aim to link the chemical process of the reaction to its impact at material level or (ii) macrostructural models which focus on the structural level assessment of affected concrete structures. Fundamental to most of these models is the assumption that ASR gets exhausted in time, which in the field, has thus far been rarely observed. In this study, a finite element model of a hydropower plant affected by ASR showing no signs of exhaustion even after 60 years of operation, was developed, validated and calibrated. From the analysis of the developed model in which a macrostructural thermo-chemo-mechanical ASR constitutive model was used to model concrete swelling, a prognostic evaluation approach to aid in determining the life expectancy of the hydropower plant was proposed.

ACKNOWLEDGEMENTS

Firstly, I would like to thank my thesis supervisor; Prof. P. Moyo, for his continuous support, guidance and valued advice towards the completion of this work. Secondly, I would like to acknowledge and thank the Uganda Electricity Generation Company Limited and their stakeholders for allowing me conduct this research using data from the Hydropower Plant they manage (Nalubaale Power Station). Additionally, I would also like to acknowledge and thank Mr K. Matongo, a senior Ph.D student, for his valued support and help throughout this research.

I would also like to acknowledge Associate Professor F. Martinez and his colleagues, Dr J. Rodriguez and Dr P. Gonzalez for providing me with their ABAQUS subroutine which they wrote specifically for the application Saouma's (2014) ASR constitutive model. Without this subroutine, this research was not going to be possible.

I would also like to acknowledge the Concrete Materials and Structural Integrity Research Unit (CoMSIRU) from the University of Cape Town for their financial support and general support throughout this study.

I would also like to acknowledge and thank Emmanuel P. Mapulanga who finished his undergraduate studies in 2015 for his help and support.

A special thanks goes to:

The National Research Fund (NRF) for providing financial support

Everyone in the Department of Civil Engineering in the University of Cape Town for striving towards providing a conducive environment for students to study;

Last but not least, all the students supervised by Prof Moyo for the indirect support you have provided.

Computations were performed using facilities provided by the University of Cape Town's ICTS High Performance Computing team: *http://hpc.uct.ac.za*.

TABLE OF CONTENTS

LIST OF FIGURES

LIST OF TABLES

NOMENCLATURE

Latin Upper Case

ASR Alkali Silica Reaction

COD Crack Opening Displacement

E Material elastic modulus

FEM Finite Element Method

RH Relative Humidity

T Temperature

Latin Lower Case

cr Cracking

el Elastic

in Inelastic

pl Plastic

x, y, z Cartesian coordinate system

Greek Lower Case

ε strain

ϵ volumetric strain

ξ expansion

σ stress

GLOSSARY

Mitigation – includes actions that seek to reduce the severity of deterioration

Calibration – involves adjusting model parameters to maximise its agreement with field test results

Diagnosis – involves the identification of the nature or cause of structural deterioration deteriorating

Prognosis – involves predicting the potential for future expansion and/or resulting further deterioration

Validation – includes comparing the field test results with the model results to quantify the accuracy of the model to represent the real

Amorphous – refers to highly disordered crystalline structure

Hygroscopic – tends to absorb water from surrounding

Structural Deterioration – includes the process of progressive loss or reduction in resistance of a structure to structural loads

Maintenance – involves preventing unnecessary deterioration (i.e. trying to preserve a certain condition or functionality)

Morphology – includes characteristics that define particles like size shape and/or structure

1 INTRODUCTION

1.1 Background to Study

Numerous concrete structures such as hydropower plants, bridges and nuclear power plants have experienced severe material deterioration of concrete due to Alkali-Silica Reaction (ASR). ASR is a deleterious chemical reaction between alkalis in concrete and some silica based aggregates resulting in extensive cracking in the concrete as the reaction product of ASR is expansive over time. This extensive cracking results in the degradation of the engineering properties of the concrete including the stiffness and strength of the concrete. Consequently, many efforts have been made to investigate ASR (itself) on the material and structural scale including the structural response of concrete structures/members to ASR (Pan et al, 2012). Thus, it was observed that once the reaction initiates in a structure, there is no available method by which the reaction can be stopped. Rather, remedial/mitigation measures such as slot cutting and grouting of cracks can be used to reduce or to try and manage the risk of failure associated with ASR ((Pan et al, 2012), (Saouma, 2014)). Additionally, ASR has been assumed to come to completion/exhaustion (based on experimental studies) since it is chemical reaction. Consequently, many assessment tools which have been developed over the years have been premised on the afore mentioned assumption, including many (if not all) macroscopic constitutive models which have been developed for the realistic simulation of ASR induced expansion that seek to aid in assessing the effectiveness of any proposed remedial action ((Pan et al, 2012) among other reasons (Saouma, 2014), (Giorla, 2013)). However, the exhaustion of ASR which has been observed experimentally (mainly), is rarely observed in the field (Giorla, 2013). In this study, a hydropower plant affected by ASR and in which the reaction extent does not seem to be slowing down (leading to exhaustion of the reaction) even after 60 years in service is considered and a proposal for the estimation of its the life expectancy made proposed.

1.2 Problem Statement

Since there exists no economically feasible method to stop the reaction, there exists a need for the engineering profession and owners of different ASR affected structures to (i) understand the progression of the reaction, (ii) understand its structural implications and effect on the

structural behaviour of these structures, and (iii) be able to access the evolution in the dam structure's response to ASR and any possible planned mitigation measures in the Surveillance and Maintenance of these structures.

1.3 Objectives of the Research

The objective of this research is therefore to produce a working FEM model to simulate the expansion of concrete due to ASR based on the ASR constitutive model proposed by Saouma (2014) resulting in an in-depth understanding of the implications of the ASR on the structural behaviour (performance) of concrete structures. This research forms a sub-section of continuing research that is currently being carried out in the Surveillance and Monitoring of Concrete Dams by the Concrete Materials and Structural Integrity Research Unit (CoMSIRU) within the Civil Engineering Department at the University of Cape Town.

1.4 Scope and Limitations of the Research

This report will be limited to concrete hydropower dams. Additionally, this research will be limited to using the ASR constitutive model as was proposed by Saouma (2014). Furthermore, all the Numerical Modelling will be carried out using ABAQUS; a finite element modelling commercial package.

It should be noted that although a thermal analysis of the numerical model ideally needs to be carried out before the ASR constitutive model can be implemented, a thermal analysis of the Hydropower plant fell outside of the scope of this research and was thus not undertaken.

Further, it should also be noted that the site measurements used to calibrate this model were obtained and are thus limited to site measurements and records from different reports undertaken by researchers and consultants working on the structural assessment of the hydropower plant.

1.5 Significance of the Research

The successful implementation of this research will help in the Surveillance and Monitoring of concrete structures affected by ASR by providing practising engineers with a practical understanding of the resulting effects of ASR on the structural behaviour of concrete dams (in

this case, Nalubaale Hydropower Plant). Additionally, this research may be the first step from which an understanding of the impact of any repair and rehabilitation of the affected structure may be developed, further research being required.

1.6 Plan and Structure of the Thesis

The proposed outline of the research is as follows:

Chapter 1 – Introduction

This chapter provides the background, objectives, scope, limitations and significance of this research.

Chapter 2 – Literature Review

This chapter provides a summary of the chemistry and/or mechanism of ASR and its structural implications on concrete structures. Additionally, it provides a summary on different numerical modelling techniques that have been developed over the years.

Chapter 3 – Development of an Ageing Concrete Hydropower Dam Model

This chapter outlines and describes the procedure followed in the development of the hydropower plant's FE model in ABAQUS. Additionally, it provides a description of the material constitutive model and the ASR constitutive models (including their implementation in ABAQUS).

Chapter 4 – Results and Discussion

This chapter contains a comparison and analysis of the results from the numerical models and site investigation observations.

Chapter 5 - Conclusions and Recommendations

This chapter provides conclusions and recommendations based on the results and discussion section.

Bibliography

This section of the report provides a list of the research and/or reference work reviewed towards the successful completing of this study.

Appendices

This chapter contains an example of the input file used in ABAQUS for this study.

2 LITERATURE REVIEW

2.1 Understanding Alkali-Silica Reaction (ASR)

ASR is now recognised as a major cause of concrete deterioration around the world (US Department of Transportation, 2012). ASR and its effects was first identified and reported by Thomas Stanton of the California State Division of Highways around 1940. Stanton's studies demonstrated that the expansion of mortar bars was influenced by (i) the alkali content of the cement, (ii) the type and amount of the reactive silica aggregate, (iii) the availability of moisture and (iv) temperature (Stanton, 1940). Stanton (1940) further showed that expansion was negligible when the alkali content of the cement was below 0.60% Na_2O_e. Subsequent to Stanton's (1940) findings, ASR has been the subject of research and has been diagnosed to be the cause of deterioration of some of the world's most critical structures such as dams, hydropower plants, and nuclear power stations among others. (US Department of Transportation, 2012). The section that follows provides a summary of the mechanism, effect and evaluation of the effects due to ASR on the structural behaviour of concrete structures.

2.1.1 Chemistry and/or Mechanisms

Alkali-Silica Reaction is an acid-base reaction with silica in solid state as the acid reactant and potassium and/or sodium hydroxide in the pore solution, together with calcium hydroxide in solid state as the basic reactants. The reaction occurs in water as it's medium resulting in calcium potassium silicate hydrate, or a calcium sodium silicate hydrate as the reaction product. (Saouma, 2014). Figure1.1 is an illustration of the sequence by which the alkali-silica reaction occurs.

Firstly the concrete pore solution has to be dominated by sodium Na^+, potassium K^+ and hydroxyl OH^- ions (Figure 2.1). These alkalis (Na^+ and K^+) present initially in the anhydrous phase (i.e. in the absence of water) in the cement in the form of sodium oxide Na_2O and potassium oxide (K_2O) undergo hydration (i.e. they dissolve into the pore liquid) (equation 2.1):

$$R_2O + H_2O - 2R^+ + 2OH^- \qquad (2.1)$$

where R^+ denotes an alkali ion such as Na^+ and K^+.

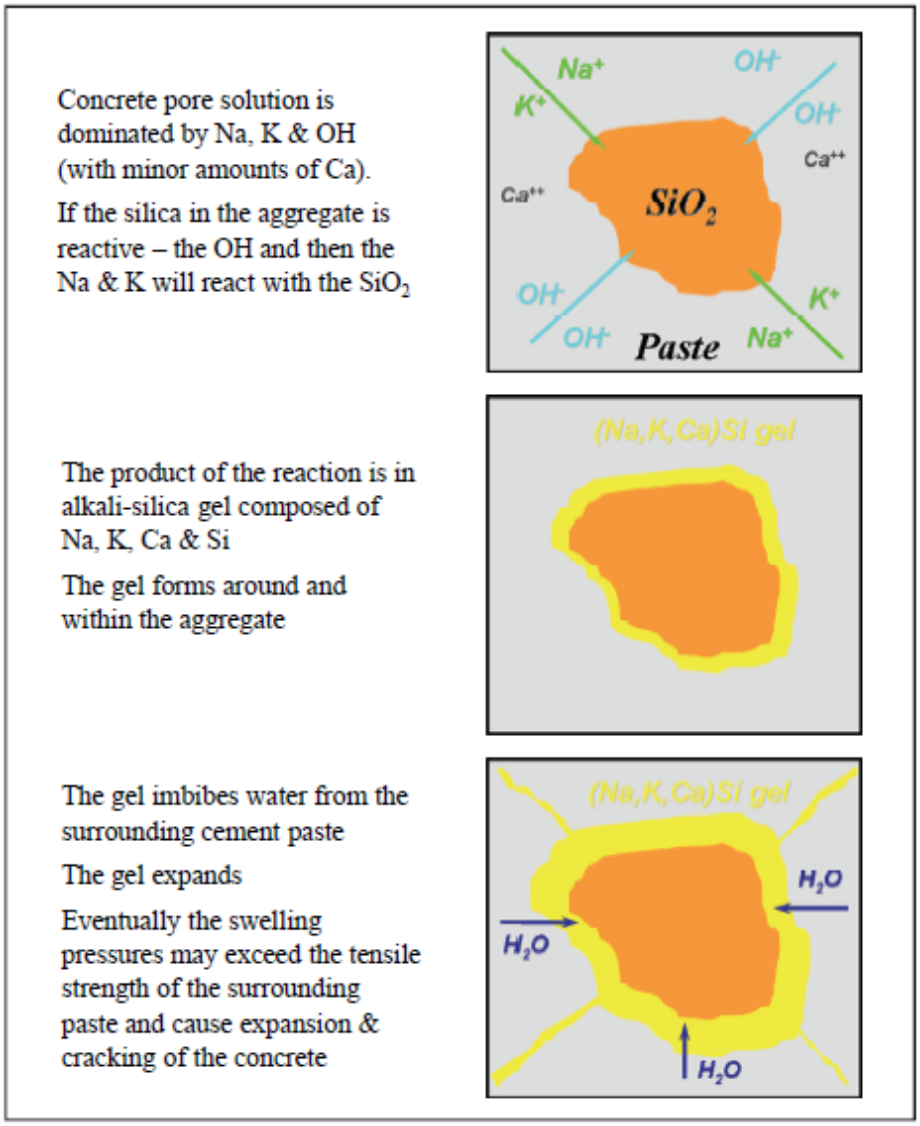

Figure 2.1: Alkali-Silica Reaction sequence (US Department of Transportation, 2012)

These alkalis are not constituents of the cement hydration process. Consequently, they accumulate in the pore solution resulting in an increase of the pore solution pH to values of typically 13.2 to 14 (due to increased concentration of hydroxyl ions (OH^-)). As already mentioned above, cement is the main and in most cases, the sole contributor of the alkalis available for the reaction to occur. However, there is increasing evidence from research that alkalis can also be found in some aggregates where they "cohabit" with silica provided the pH is below a certain critical value (Saouma, 2014). Additionally, alkalis can originate from

external sources such as de-icing salt in countries were de-icing salt is used (US Department of Transportation, 2012).

Consequent to the accumulation of alkali and hydroxyl ions in the concrete pore solution and the availability of reactive aggregate in the concrete, the alkali silica reaction (ASR) will initiate (Figure 2.1) as shown in equation 2.2:

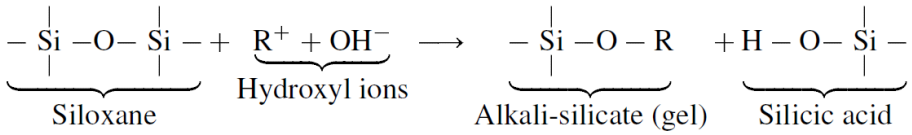

(2.2)

where R^+ denotes an alkali ion such as Na^+ and K^+.

In the manufacture of concrete, aggregates constitute 60 to 80 per cent of the volume of concrete and in most cases, these aggregates originate from parental rock sources (Ghasemi, 2017). The reactive component of concrete aggregates essential for ASR to initiate (as can be seen in equation 2.2 above) is the Silica in the aggregates. Silica (Si) comprises about 65% by weight of the accessible portions of the earth's crust. Thus, silica is the main constituent of most aggregates in the form of silicon dioxide (SiO_2) (Siloxane (equation 2.2)). It occurs in two forms namely: (i) as a solid crystalline oxide from which other elements such as aluminium, magnesium, hydrogen, etc. are absent; (ii) silicates, in which silicon and oxygen are combined with other elements such as potassium, sodium, calcium and iron, in addition to those already mentioned previously (Saouma, 2014). Most of the silicon dioxide is stable. However, some of it is poorly crystallised and is thus thermodynamically unstable with respect to its crystalline structure (Figure 2.2). Figure 2.2 schematically shows two silica minerals, opal and quart. These minerals are both similar in chemical composition (primarily being composed of SiO_2) but have different crystalline structures. Opal (Figure 2.2) has a highly disordered (amorphous) crystalline structure which renders it unstable at high pH levels (US Department of Transportation, 2012).

On the other hand, quartz (Figure 2.2), has a highly ordered and thus stable crystalline structure. Consequently, aggregates containing significant quantities of the mineral opal and/or minerals with like crystalline structures may be reactive when used in concrete with sufficient alkali content (the poorly crystallised silica are prone to react with the hydroxyl ions on the surface

of the aggregate to produce silanols (Si-OH groups)), whereas quartz and/or minerals with similar crystalline structures are expected not to react deleteriously regardless of the alkali content of the concrete. (US Department of Transportation, 2012).

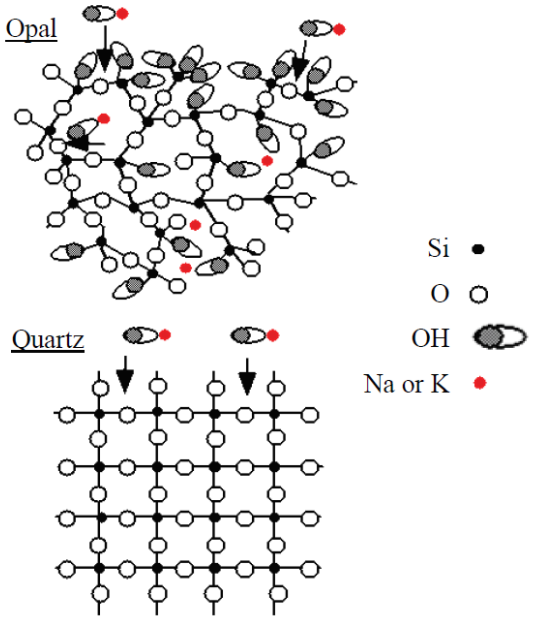

Figure 2.2: Schematic showing the crystalline structure of Opal and Quartz Minerals (US Department of Transportation, 2012)

The silicic acid formed in the hydrolysis of the siloxane (Si-O-Si) is weak and therefore immediately reacts with the hydroxyl ions resulting in water and a negatively charged Si-O- as the reaction products. The readily available and abundant alkali ions in aqueous state diffuse into the gel to balance the negatively charged species (illustrated in equation 2.3).

$$\underbrace{H-O-\overset{|}{Si}-}_{\text{Silicic acid}} + \underbrace{R^+ + OH^-}_{\text{Hydroxyl ions}} \longrightarrow \underbrace{-\overset{|}{Si}-O-R}_{\text{Alkali silicate (gel)}} + \underbrace{H_2O}_{\text{Water}} \qquad (2.3)$$

The resultant alkali-silicate (alkali silica gel) precipitates in the presence of calcium (Ca). Else, if calcium is not available in the pore solution, the reactive silica dissolves in the alkali hydroxide solution without the alkali silica gel expanding ((Diamond 1989) (Thomas & Bleszynski (1998)). Although the precise role(s) of $Ca(OH)_2$ is not clear, it is evident that calcium must be available for significant expansion (expansion which results in structural

degradation and deterioration (damage)) of the Alkali-silicate gel to occur (Figure 2.1) (US Department of Transportation, 2012).

The Alkali silicate precipitate (alkali silica gel) is hygroscopic (expansive in the presence of water) and forms around the aggregate (Figure 2.1) except for R = Lithium.

$$\underbrace{-\overset{|}{\underset{|}{Si}}-O-R}_{\text{Alkali-silicate (gel)}} + \underbrace{nH_2O}_{\text{Water}} \longrightarrow \underbrace{-\overset{|}{\underset{|}{Si}}-O^- + (H_2O)_n + R^+}_{\text{Expanded alkali silicate (gel)}} \qquad (2.4)$$

(Equation 2.2 to 2.4 follow the notation as was illustrated by Saouma (2014))

Thus, in the presence of water the alkali silica gel expands by absorbing water (chemically represented in equation 2.4). The expansion of the gel results in eventual swelling pressures which may exceed the tensile strength of the surrounding paste causing expansion and cracking of the concrete (Figure 2.3) (i.e. concrete damage) (US Department of Transportation, 2012).

Initially, as the alkali silica gel absorbs water and expands, it fills all the available space such as voids and/or cracks. Eventually the swelling pressures may exceed the tensile strength of the surrounding paste resulting in expansion and cracking of the paste and/or aggregates (Figure 2.1). As the concrete expands from within outwards, two main zones separated by a third expansion zone in the concrete develop (Figure 2.3a). The first zone, the central zone, is characterised by random micro cracks due to the tensile strength of the paste and/or aggregate being exceeded (Figure 2.3). The second layer, the surface layer is characterised by random macro cracks that develop in a direction normal to the surface (these surface cracks are usually described as map cracking). However, the cracking pattern on the surface layer can vary depending on the restraint and/or loading conditions to which the surface is exposed. The third zone which separates the central zone and the surface zone develops due to the reduction in internal restraint normal to the surface. Consequently, the micro cracks in the third zone develop sub parallel to the surface (Figure 2.3).

The expansion and cracking (i.e. deleterious expansion) of the concrete due to ASR leads to the structural degradation and deterioration of the concrete. However, deleterious expansion of concrete could be prevented if the alkali content of the concrete was kept below 3.0 kg/m^3 Na_2Oe (Thomas et al, 2006). The alkali content of the concrete is of more importance when it

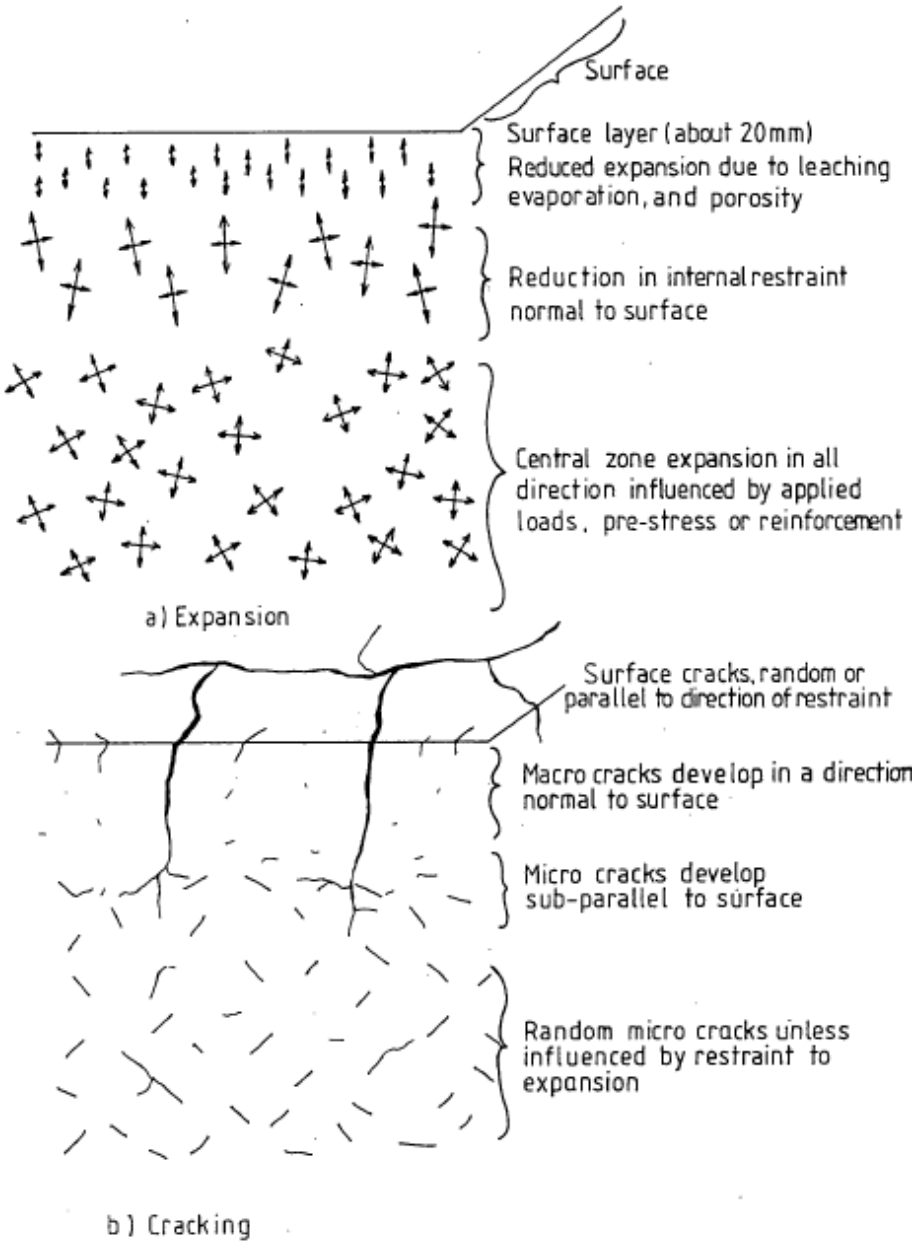

Figure 2.3: Schematic showing the development of cracking due to ASR (McLeish, 1990)

comes to preventing ASR from initiating as there can be other sources of alkalis in the concrete throughout a structures service life such as (i) alkali migration caused by moisture movements or electrical currents, (ii) penetration of alkalis from external sources (e.g. de-icing salts), or (ii) long-term release of alkali from aggregate. (US Department of Transportation, 2012).

In the field however, expansion is anticipated to occur at lower alkali contents than the value of 3.0 kg/m^3 Na_2Oe Thomas et al (2006) specified because the value they specified was based on laboratory tests. Laboratory tests have the disadvantage that the largest size of test specimen

testable are usually too small for realistic measurements to be made to assess realistic structure (Blight and Alexander, 2011). Thus, main factors that affect the reaction progression like the leaching of the alkalis, on real structures (Figure2.4) does not occur to the same scale as the concrete laboratory test specimens (US Department of Transportation, 2012).

Figure 2.4 illustrates surface discolouration and gel exudations (leaching) due to ASR.

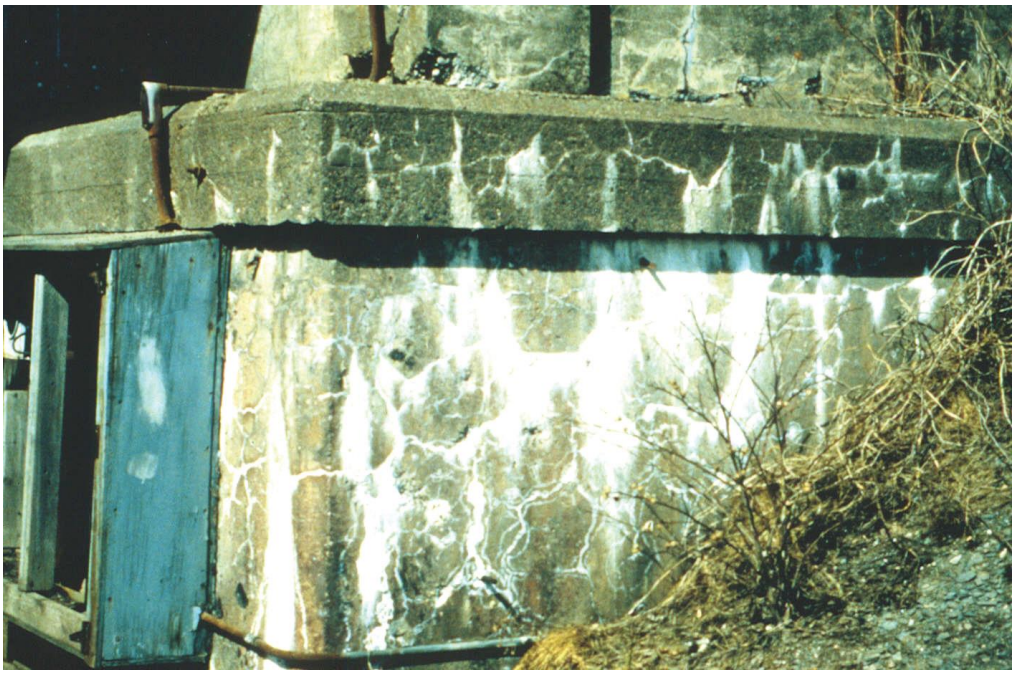

Figure 2.4: Efflorescence and exudations of ASR at the surface of a 25 year old highway bridge concrete foundation (US Department of Transportation, 2012)

Additionally, it is generally acknowledged that the chemical reaction will cease if the internal relative humidity inside the concrete falls below 80%. This is because, sufficient moisture is required to both sustain the chemical reaction and to provide for the expansion of the gel. Thus local differences in the moisture availability within the same structure can result in very different levels of ASR damage occurring within the same structure (US Department of Transportation, 2012).

2.1.2 Effects of ASR (Diagnostic Structural implications)

The deterioration of concrete due to ASR is observable through (i) the expansion of the material and (ii) the degradation of its mechanical characteristics. The expansion of the material is directly induced by the swelling of the reaction product (alkali silica gel) and may result in the development of differential internal stresses, possible dimensional increases and interaction of

the ASR affected structural members with other less affected or non-affected structural members. Consequently, the development of differential internal stresses results in internal and external cracking (Figure 2.3). Observable external cracks (consequent to the differential internal stress) are usually randomly-oriented on the surface of concrete elements. These randomly oriented cracks are known as map cracking or pattern cracking (Figure 2.5).

Figure 2.5: Map cracking and associated gel staining around cracks in a median highway barrier affected by ASR (US Department of Transportation, 2012)

Additionally, confining stresses (in cases where confining stresses might exit) due to the expansion restraint which may be caused by reinforcement for example, may result in the development of differential internal stress distributions within the structure. Consequently, the external observable cracks may develop parallel to the confining stress (Figure 2.6 shows externally observable cracks on the column aligned vertically due to restraint imposed by the primary reinforcement and dead load).

Figure 2.6: Preferred alignment of cracks in an ASR-affected concrete column (US Department of Transportation, 2012)

Further, the expansion of the material results in dimensional increases of a structure. These dimensional increases can lead to observable deformation on structural members either due to the dimension increase and/or due to the resulting interaction of the ASR affected structural member with other less affected or non-affected structural elements (Figure 2.8).

Figure 2.7 Relative movement of abutting sections of parapet wall in a bridge structure (US Department of Transportation, 2012)

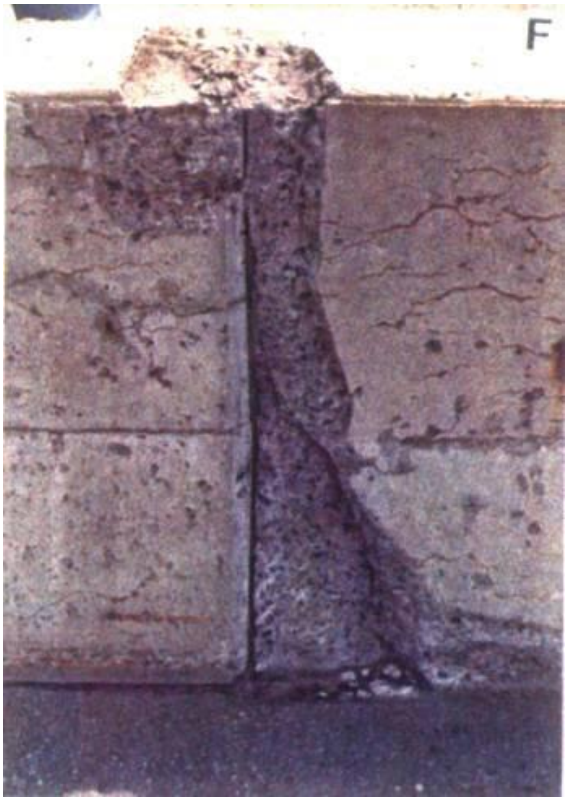

Figure 2.8: Severe spalling associated with expansion due to ASR in abutting barrier section (US Department of Transportation, 2012)

Furthermore, the extent of ASR often varies between and/or within different structural elements of a concrete structure, resulting in relative movement (displacements) of adjacent concrete members or structural units (Figure 2.7). This relative movement may result in excessive deflections and/or closure of joints, as well as spalling of concrete at joints (Figure 2.8). Additionally, the combined effect of differential stress distribution with dimension increase and/or structural member interaction may also result in localised crushing of the concrete (Figure 2.9).

On the other hand, the deterioration of the material mechanical properties of concrete is consequent to the cracks forming within the aggregates and/or cement paste (micro cracking process). Generally, for unrestrained concrete specimens, both the strength and stiffness of the concrete are reduced. Although the trend in the degradation of the engineering properties of unrestrained concrete specimen is still unknown, the elastic modulus is the most affected property, followed by the tensile strength. The least affected engineering property is the

compressive strength. ((Esposito, 2016); (Clark, 1989)). Since ASR related expansions are sensitive to the stress state of the affected concrete, the deterioration in the strength and

Figure 2.9: Expansion of bridge girder leading to loss of clearance between the girder and embankment and eventual crushing of girder (US Department of Transportation, 2012)

stiffness (above discussed) for unrestrained concrete specimen are not perfectly and exactly replicated from load tests on structures badly affected by ASR. To the contrary, the load tests indicated no significant effect of ASR deterioration on either the strength or stiffness (Clark, 1989). The difference in the degradation trends of the engineering properties of concrete from laboratory tests to those from load tests on real structure can be attributed to the fact that concrete in a structure is subject to restraint by adjacent material and/or reinforcement. Clark (1989) noted that reinforcement detailing has a significant effect on the response of a structure to ASR expansion including the deterioration of the mechanical properties of the concrete. Furthermore, Clark (1989) also noted that concrete affected by ASR becomes more ductile with a greater strain at peak stress and also with no reduction in the ultimate strain capacity (Clark, 1989). Another mechanical property of concrete that is especially important for reinforced concrete and that may also be degraded by ASR is the bond strength (Dolen, 2005).

2.2 Constitutive models of ASR

ASR models fall into two main categories (Giorla, 2013):

(i) Macro-structural models which have been developed for the analysis of large concrete structures affected by the ASR and,

(ii) Microstructural models which aim to link the chemical process of the reaction to its impact at the material level.

Although other finely refined classifications of ASR related constitutive models exist, for example Saouma (2014) provides three main categories of ASR expansion models namely: (i) micro models, (ii) meso models, and (iii) macro models, this review will focus on two main categories differentiated whereby the models are differentiated by the purpose of their development, namely: macro-structural models, which are largely developed for the analysis of large structure and micro-structural models which are largely developed for the analysis of the concrete's micro structural processes of the reaction.

2.2.1 Macro-structural models

Macro-structural models require the input of a wide range of properties which depend on the material microstructure and cannot be explicitly represented at this scale. These material microstructural properties include the imposed expansion, water flows, etc. Consequently, macroscopic constitutive laws that can either be empirically derived from the fitting of curves from experimental observations, or from multi-scale models (which are based on the knowledge of the physical processes at the micro-scale), have been developed to approximate these physical processes (which include water flows, creep, and imposed expansion) that occur within the material. In most of these models, the expansion and/or degree of reaction are typically expressed as a sigmoidal functions of time based on the free expansion measured experimentally (Figure 2.10). (Giorla, 2013).

There exist three classifications for macro-structural, namely: (i) Phenomenological models, (ii) Poro-mechanical models, and (iii) Reaction rims models (Giorla, 2013). These classifications differentiate macro-structural models based upon how each model represents the Alkali Silica gel.

Figure 2.10 below is an illustration of the sigmoid function showing the aforementioned parameters that characterise this graph.

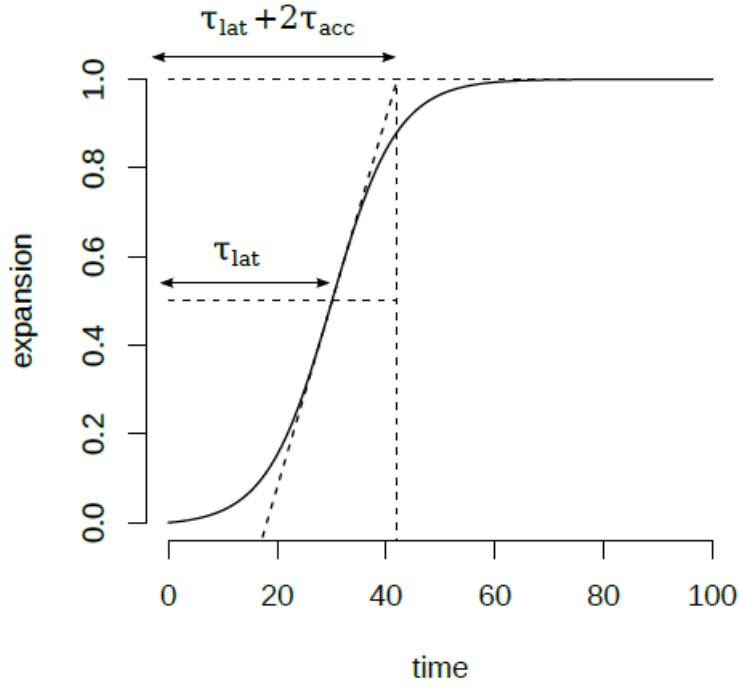

Figure 2.10: Expansion modelled as a sigmoidal function of time (Giorla, 2013)

Phenomenological models:

In phenomenological models the ASR expansion and induced damage are simulated from macroscopic laws derived from experimental measurements. The earliest models from this classification modelled the ASR expansion as uniformly distributed in the concrete structure because it was easier to impose an equivalent homogeneous thermal load rather than deriving and implementing a specific constitutive law (Giorla, 2013). These models were later refined by varying the imposed expansion across the structure as a function of the relative humidity, temperature, compressive stresses or concentration of reactive components among other factors. For example, Bazant & Steffens (2000) or Capra & Bournazel (1998), accounted for the reduction in the final expansion due to a decrease in the saturation degree (observed experimentally) by a factor between 0 and 1 that depends on the degree of saturation in the material (Giorla, 2013). Furthermore, these models use three main parameters: (i) the asymptotic expansion ($\varepsilon_{ASR}^{\infty}$) which controls the amplitude of the deformation, (ii) the latency (τ_{lat}) which controls the induction period of the reaction, and (iii) the acceleration characteristic

time (τ_{acc}) which controls the main slope of the sigmoid (Figure 2.10) ((Saouma & Perotti, 2006) (Giorla, 2013)).

Poro-mechanical models:

On the other hand, Poro-mechanical models are based on the assumption that the expansive silica gel forms inside the concrete pores. As already alluded to and similarly to phenomenological models, the amount of gel formed is assumed to follow a sigmoidal function of time to reflect the experimental expansion curves. Further, the macroscopic expansion is assumed to translate from the pressure exerted by the reaction gel on the pore walls. The macroscopic constitutive material law that governs the reaction extent and structural effect of ASR on the concrete in poro-mechanical models is described in equation 2.5:

$$\sigma = \mathbb{C}: \varepsilon + \mathbb{B}: \sigma_{ASR} \quad (2.5)$$

where $\mathbb{B}$ is equivalent to the Biot tensor used in poro-mechanics (Biot, 1955) and refers to the amount of gel-filled pores and their geometry, and σ_{ASR} is the pressure imposed by the gel.

These two parameters ($\mathbb{B}$, σ_{ASR}) correspond to an idealisation of the material microstructure (e.g. the amount of porosity accessible to the gel and/or the geometry of the pores) which cannot be measured experimentally but can be fitted for a specific concrete mix and/or can be derived using analytical homogenisation schemes. For example, Li (2002) assumed that the pores in which the reaction gel formed where ellipsoidal. He further assumed that the aspect ratio of these pores changed as the reaction progressed because of micro-cracking. Consequently, $\mathbb{B}$ changes as the cracks propagate (Li, 2000). Although Li (2000) found that he could reproduce the trends observed by Larive (1997) with respect to uniaxial expansion, his model could not account for the change in the aspect ratio as the reaction advanced. Capra & Sellier (2003) on the other hand, used the gel pressure to estimate the damage caused by ASR. They identified a way to describe their model using $V_{accessible}$, σ_{ASR}, V_{gel}, V_{cracks} and the global tensor, ε, based on assumptions made of the microstructure of the affected concrete by substituted the aforementioned terms in equation 2.5 (Capra & Sellier, 2003). Further, they also assumed that the gel fills the accessible pores before it can exert pressure on the solid skeleton, resulting in delay in the observed expansion (Capra & Sellier, 2003). However, similarly to Li's (2000) model, similar coefficients (as those used in equation 2.5) based on assumptions about the microstructure of the ASR affected concrete were used in Capra & Sellier's (2003).

Consequently, the coefficients used in Capra & Sellier (2003)'s model have to be calibrated for each experimental set as they cannot be measured experimentally. Various other researchers such as Grimal et al (2010) and Bangert et al (2004) proposed variants of poro-mechanical models. However, poro-mechanical models typically rely on a number of parameters which are impossible to measure experimentally. Consequently, these models require a large number of fitting parameters and are thus mix or experimental set dependant, among other draw backs (Giorla, 2013).

Reaction rim models:

Reaction rim models were developed to propose a better representation of the microstructure. Each aggregate is considered separately in a representative elementary volume (REV) of cement paste. Additionally, the reaction is assumed to occur around the aggregates in the interfacial transition zone (ITZ). Bazant et al (2000) divided his proposed model into a chemical component which controlled the rate of reaction, and a fracture mechanics component which described the cracking of the cement paste. In the aforementioned model, the overall isotropic expansion is obtained by integrating over all possible crack orientations and the cracks are assumed to develop around each aggregate. However, Bazant et al (2000)'s model does not consider the interaction between each crack. Additionally, his proposed model fails to represent the loss in compressive or tensile strength because the model is not well suited to capture expansion from slow reactive aggregates (the majority of aggregates used in the field are slow reactive aggregates). On the contrary, the model is well suited to capture expansion due to highly reactive aggregates such as opal (Giorla, 2013). In contrast to Bazant et al (2000)'s proposed model, Charpin's (2013) proposed a model that considered different fracture mechanisms such as debonding around the aggregate and propagation of cracks in three orthogonal directions, occurring simultaneously around the aggregate. Further, Charpin (2013) accounted for the particle size distribution using the homogenisation approach and also accounted for the change in the morphology of the microstructure due to crack propagation. However, the model proposed by Charpin (2013) resulted in the overestimation of the debonding of the aggregate but underestimated the overall expansion. Giorla (2013) argued that the aforementioned discrepancies were a result of the fact that the morphology of the reaction and the crack propagation were ill-represented in Charpin (2013)'s model. Giorla (2013) further argued that the model which Charpin (2013) proposed did not account for creep and the cement

paste material was assumed to be purely elastic instead of visco-elastic, resulting in the overestimation of the damage (Giorla, 2013).

2.2.2 Micro-structural models

Microstructural models describe explicitly the concrete microstructure and are usually developed for the analysis of laboratory experiments. Consequently, the modelling efforts are focused on a few select phenomenon since only a limited number of parameters can be varied in experimental investigations. However, these models (micro-structural models) are useful in understanding the mechanisms of ASR and also help in the construction of macroscopic constitutive laws. The location at which the alkali silica gel is assumed to form is an important parameter in these models as it detects where the cracks initiate and how they propagate. Expanding aggregate models and gel pocket models are two type of micro-structural models characterised based on the location of gel formation. In the expanding gel models, the expansion results either from the gel forming around the aggregate (similar to reaction rim models) or by homogeneous expansion of the aggregates themselves ((Schlangen & Copuroglu, 2007) (Comby-Peyrot et al, 2009)). On the other hand researchers such as Dunant & Scrivener (2010) have proposed models in which the expansion is caused by gel pockets in the aggregate and/or paste (gel pocket models). Of the two micro-structural models, gel pocket models seem to give the best correlation between experimental data and numerical simulation (Giorla, 2013).

Additionally, other factors influence the micro-cracking process, such as the the particle size distribution and/or shape of aggregates (circular or ellipsoidal). These other factors are usually analysed using micro-structural models. One such model which can be used to investigate these morphological parameters (e.g. gel location and shape of the aggregates) is the model proposed by Dunant (2009). Dunant,(2009) showed that the expansion caused by circular aggregates is isotropic and the expansion resulting from ellipsoidal aggregates is anisotropic resulting in similar expansion trends to those observed in experimental studies (Giorla, 2013).

2.3 Chapter Summary

In summary, for degrading ASR to occur there needs to be a sufficient quantity of reactive silica, a sufficient concentration of alkalis and sufficient moisture. The degradation of the concrete results from the expansion of the reaction product, which causes micro-cracking of the concrete and also leads to the degradation of the concretes mechanical properties. Further, the

expansion also causes other diagnostic characteristics of ASR such as surface cracking, excessive deformations and gel exudation. Thus, to understand the reaction mechanism and to aid in the assessment maintenance of ASR affected structures different modelling approaches have been proposed. Most of the proposed models can be categorised based on where the reaction product and is assumed to be formed and the type of analysis for which they have been developed (i.e. microstructural analysis or overall macro structural evaluations).

3 DEVELOPMENT OF AN AGEING CONCRETE HYDROPOWER DAM MODEL

3.1 Introduction

Nalubaale Hydropower Station formerly known as Owen falls Dam consists of a power station with an installed power generation capacity of 180MW alongside a mass concrete gravity dam about 30 metres high and 800 metres long. It is located approximately 3 kms downstream from Lake Victoria on the Nile River in Jinja (Uganda) (refer to Figure 3.1) and is owned by the Uganda Electricity Generation Company Limited (Westlake et al, 1954).

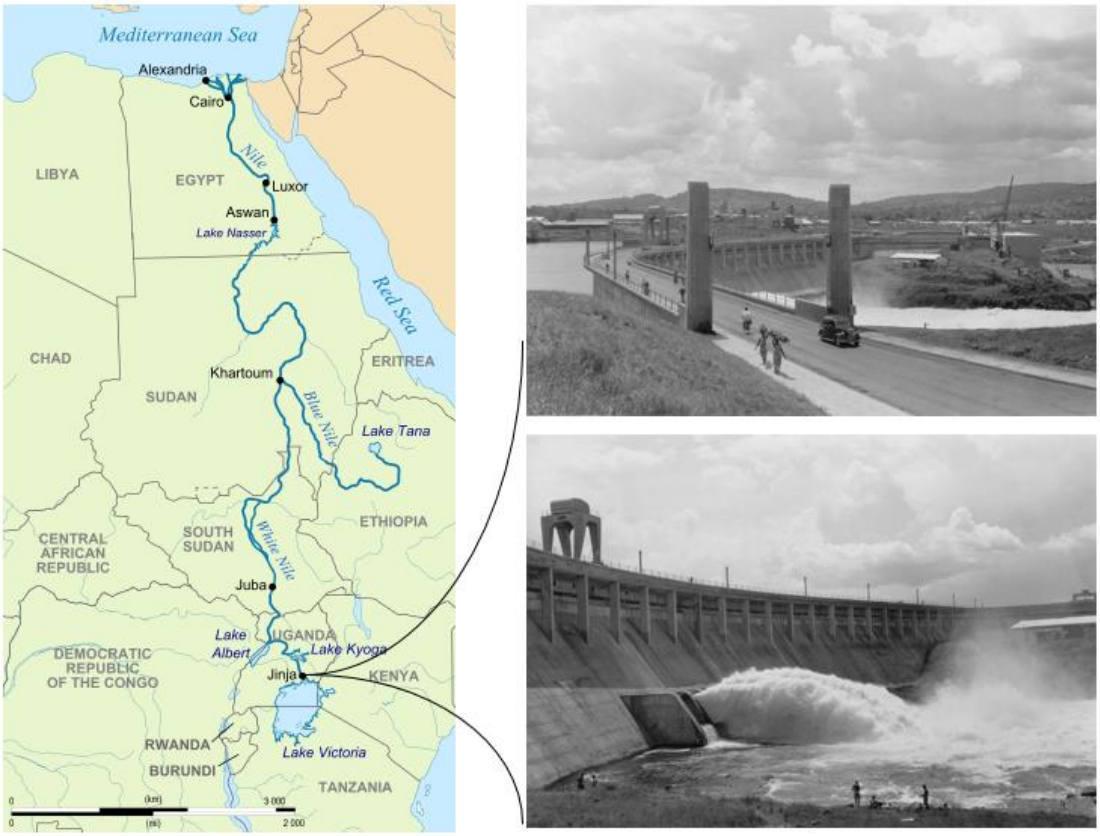

Figure 3.1: Location of the Nalubaale Power Station on the River Nile basin (https://en.wikipedia.org & http://mapio.net, 16/10/2017)

The right images in Figure 3.1 above shows the Dam in 1954. The power station has provided majority of the power in Uganda including additional power for export.

3.2 Brief History of Nalubaale Hydropower Plant

Construction of Nalubaale Hydropower Plant Complex started in 1951. The hydropower plant has ten turbines which were commissioned in stages, with the first two commissioned by 1954 and the last turbine commissioned in 1968. This provided a total installed power generation capacity of 150MW. Figure 3.2 shows the downstream view of the power station whilst Figure 3.3 shows the internal view of the generator housing units.

Figure 3.2: Downstream view of Nalubaale Hydropower Plant

Cracking in the plant was first noticed in the concrete around the fourth generator housing in 1964. During the same year, Lake Victoria which was impounded by the dam and power station reached record water rise levels of more than 2 m above those previously observed since the water level monitoring began 1896. Consequently, the coincidence of the observed cracks on the forth generator housing and the record rise in the water level resulted in the inevitable suspicion that some form of structural distress due to increased loading on the structure had taken place. Furthermore, during the 1970s, the hydropower plant deteriorated rapidly as Uganda passed through a period of political instability, firstly though the Amin regime (1971-

1979) and then through the Obote regime (1980-1985). Consequently, the plant was not inspected by the engineers who designed it until 1983.

In the 1983 inspections, the design engineers found that most turbines were operable at reduced load due to lack of spares and maintenance. They also discovered that the cracking in the power station had increased significantly, including a major crack that run through the length of the machine hall floor (Figure 3.4) and the cracking in generator housing machine No.4 had increased and was mirrored at all other machines housings (Mason & Molyneux, 1998).

Figure 3.3: View down the Generator Housing Hall

Additionally, the design engineers found that there was some machine misalignments, clearance loses and that the local staff had installed crack gauges in 1973 to monitor crack development and had also installed targets in 1978 to monitor the downstream wall movements (Mason & Molyneux, 1998).

Figure 3.4: View of the longitudinal crack in the machine hall floor

Consequent to the inspection, some refurbishment work was started in 1988 which included (i) re-waterproofing the roof, (ii) underwater repairs throughout the plant, (iii) stressed anchoring in the power station to stabilize the structure and (iv) general refurbishment of the mechanical

and electrical equipment. Additionally, the generators were uprated to 18MW each, increasing the total capacity of the station to 180MW (Mason & Molyneux, 1998).

Continued monitoring of the cracks during the 1990s indicated that movement of the structure had not ceased and that the underlying cause of the deterioration might have been other than structural load. The crack opening monitoring seemed to suggest a linear trend since 1973 and did not seem to vary with changes in the intake level. In the 1983 inspection, the potential for structural distress due to any form of Alkali-Silica reaction was assessed from samples of spalled concrete, but had proved negative. However, the diagnosis of alkali-silica reaction was eventually confirmed by concrete analysis and structural intuitive analysis in the following years (Mason & Molyneux, 1998).

3.3 Developing the Hydropower plant geometry

The first stage in undertaking this study was to develop a 3-dimensional model of the Hydropower plant. Figure 3.5 shows a typical cross-section through the power plant. As already highlighted in section 1.4 of this report, the numerical simulation was run using ABAQUS. The Plant's geometry proved complicated to be developed in ABAQUS.

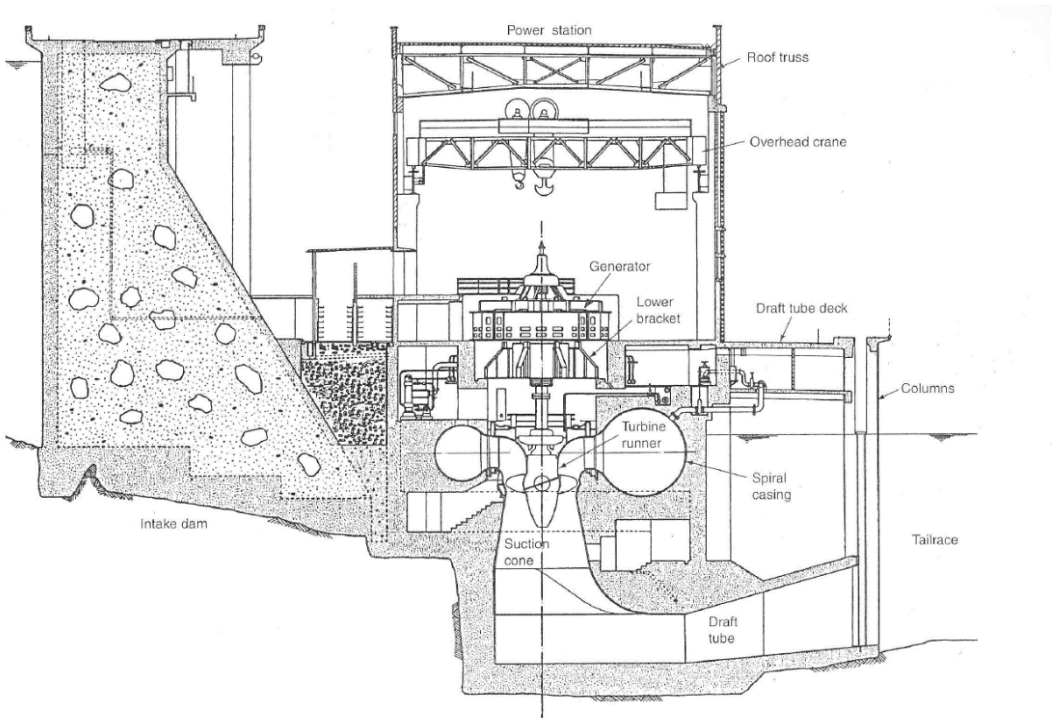

Figure 3.5: Typical cross-section through the power plant

Consequently it was developed using SOLIDWORKS, then imported into ABAQUS. Figure 3.6 shows the developed model of initially one unit and then the combined 10 units used in the analysis.

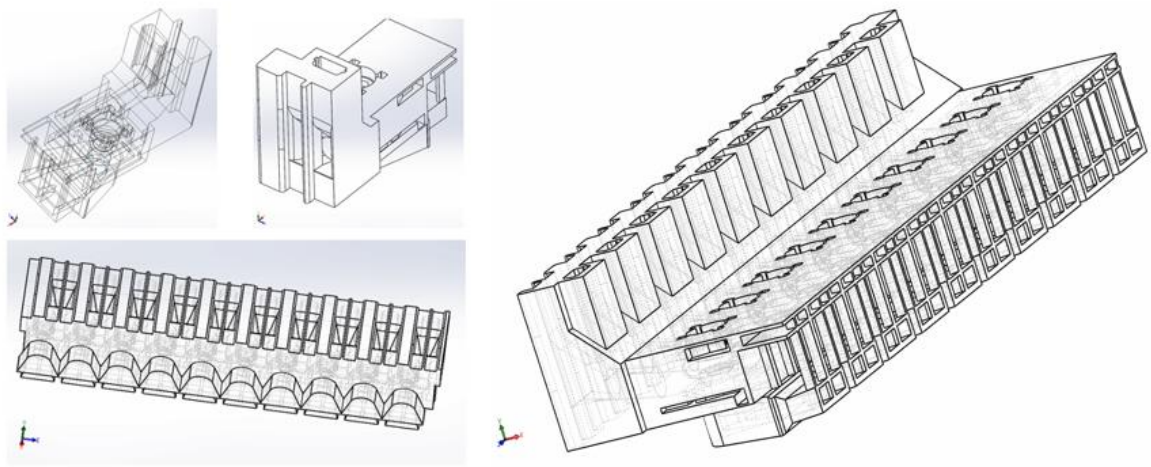

Figure 3.6: Hydropower plant geometry development

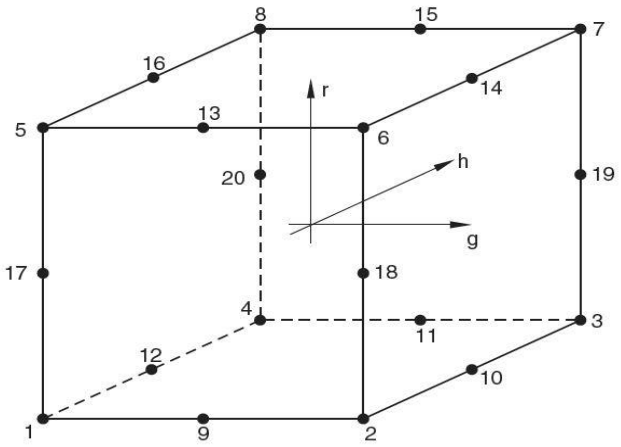

Figure 3.7: 20-node isoparametric master element (Dassault Systems Simulia Corp, 2012)

Another aspect of the model that proved a challenge to achieve because of the complexity of the geometry was the meshing. Brick elements (i.e. hexahedral three dimensional elements (Figure 3.7)) seem to give the best results when modelling concrete dams as these elements are isoparametric (Dassault Systems Simulia Corp, 2012). However, using these brick elements to

mesh the provided geometry proved impossible. Consequently, tetrahedral elements (Figure 3.8) which are generally used in simulations of incompressible materials, were used in this study. Figure 3.9 shows the complete meshed power plant model.

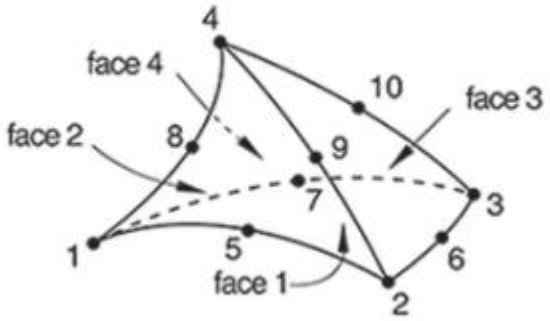

Figure 3.8: 10-node tetrahedral element (Dassault Systems Simulia Corp, 2012)

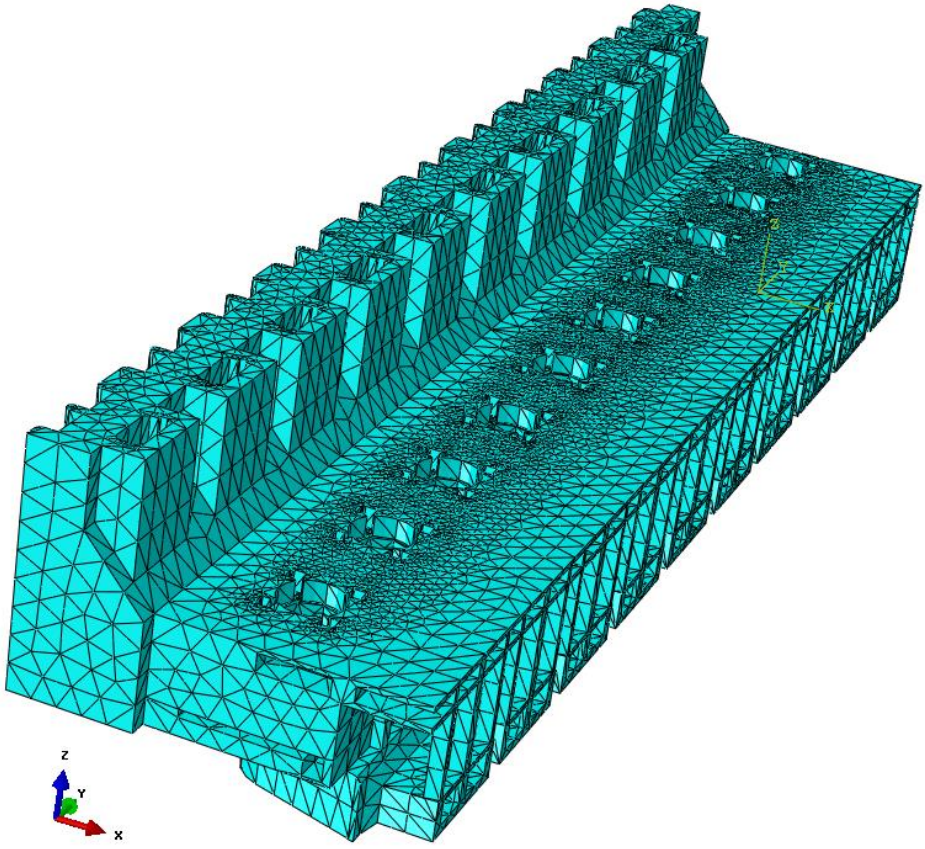

Figure 3.9: Meshed Hydropower plant geometry in ABAQUS

3.4 Defining Material Properties

(The material properties were defined and the discussion in this section relies heavily on the research undertaken by Mundeli & Moyo)

The behaviour of concrete is generally nonlinear because of the weak Interfacial transition zone between the paste and aggregate, and also due to the porosity of concrete. Simply put, the behaviour of concrete depends on its microstructure (Mundeli & Moyo, 2014). Concrete generally behaves differently in compression as compared to tension. Additionally, cracking in the concrete which may result from shrinkage, external loading, deterioration of the concrete and so on, reduces the stiffness of concrete and this is known as tensile damage. Thus concrete can be classified as a complex material. Consequently, different researchers have developed different material models for concrete to predict its response to a variety of loading situations. In this study, the Concrete Damage plasticity model as was proposed by Lubliner et al (1989) and as applied in ABAQUS was used. As its name suggests, this model combines plasticity and damage in describing the behaviour of concrete under different loading conditions.

(Please note that the discussion of different proposed material models has not been included in this study as it does not form part of the scope of the study. However, following on work done by Mundeli & Moyo (2014), the best model which is available in ABAQUS for nonlinear analysis of concrete and for the purposes of crack observation was the Concrete Damage Plasticity (CDP) model).

Generally, plasticity models; are described by three key rules (i) yield criterion, (ii) flow rule and (iii) hardening rule. Additionally, when plasticity models used alone, they do not capture the stiffness degradation of the material. On the other hand, damage models do not suitably describe both the irreversible and volumetric expansion observed in compression.

The Concrete Damage Plasticity (CDP) model assumes that concrete mainly fails in tension by cracking and in compression by crushing. The model decouples the total strain increment into elastic and inelastic components as follows:

$$\varepsilon = \varepsilon^{el} + \varepsilon^{pl} \tag{3.1}$$

$$\sigma = E : (\varepsilon - \varepsilon^{pl}) \tag{3.2}$$

where ε is the total strain tensor, ε^{el} is the elastic strain tensor, ε^{pl} is the plastic strain tensor, σ is the stress tensor and E the elastic stiffness tensor.

Adding the scalar damage stiffness degradation results in equation 3.3 below:

$$E = (1 - D)\, E_0 \tag{3.3}$$

where E_0 is the initial elastic stiffness (undamaged) and D the damage variable which varies from 0 to 1, representing an undamaged to completely damaged material respectively.

Combining equations 3.2 and 3.3 leads to the following general stress strain relationship

$$\sigma = (1 - D)\, E_0 : (\varepsilon - \varepsilon^{pl}) \tag{3.4}$$

The implementation of the CDP model in this study is summarised in Table 3.1, which provides a list of the concrete properties used in this study.

Table 3.1: Concrete material properties used in this study

Property name	Replacement Level required (%)
Compressive Strength	48 MPa
Tensile Strength	3.5 MPa
Elastic Modulus	35 GPa
Density	2400 $^{kg}/_{m^3}$
Poison's ratio	0.2

As already mentioned, concrete behaves as a plastic material when it is subjected to multiaxial stress state. Additionally, its elastic properties get damaged due to cracking of the concrete, resulting in the degradation of its stiffness and a nonlinear repsonse. This nonlinear response was determined in this study using the relationship given in the BS EN 1992-1-1 (Eurocode 2, 2004: 33, 3.1.50, similar to the parameters and model used by Mundeli & Moyo (2014)).

$$\frac{\sigma_c}{f_{cm}} = \frac{k\eta - \eta^2}{1 + (k-2)} \tag{3.5}$$

where $\eta = \frac{\varepsilon_c}{\varepsilon_{c1}}$, with ε_{cl} as the strain at peak stress given by $\varepsilon_{c1} = 0.7\, f_{cm}^{0.31} \leq 2.8\, {}^{o}/_{oo}$, ε_c is the strain in the concrete and $k = 1.05\, \frac{|\varepsilon_{c1}|}{f_{cm}}$.

The expression (equation 3.5) provides the basis for the input data used in this study in ABAQUS to describe the compressive behaviour of the concrete.

Additionally, the implementation of the CDP model requires the use of inelastic strains to describe the compressive behaviour of concrete. These strains where calculated as the difference between the total strain and the elastic strain corresponding to the undamaged material (equation 3.6).

$$\varepsilon^{in} = \varepsilon_c - \frac{\sigma_c}{E_0} \tag{3.6}$$

where the subscript c refers to compression, thus σ_c, is the stress in the concrete and $\varepsilon_c$the strain in the concrete and ε^{in} the inelastic strain.

Following from the above discussions, table 3.2 provides a summary of the nonlinear behaviour characteristics inputted in ABAQUS.

Table 3.2: Stress strain input values for compressive behaviour used in the study

Yield Stress [MPa]	Inelastic Strain
19.2	0.0E+00
29.6	4.0E-04
38.5	8.0E-04
44.6	1.2E-03
47.7	1.6E-03
47.2	2.0E-03
42.5	2.4E-03
32.7	2.8E-03
16.8	3.2E-03

To describe and define the tensile behaviour in ABAQUS, the cracking strain for each corresponding yield stress is required.

Similar to the values used by Mundeli & Moyo (2014), Table 3.3 shows the stress strain values used in the study assuming that the cracking strain at the onset of cracking is zero and the that the total strain is $\varepsilon_{cr} = \frac{f_{tm}}{E} = 0.0001$.

Table 3.3: Stress strain input values for tensile behaviour used in the study

Yield Stress [MPa]	Cracking Strain
3.5	0.0E+00
3.1	1.11E-04
2.7	2.22E-04
2.3	3.33E-04
2.0	4.44E-04
1.6	5.55E-04
1.2	6.67E-04
0.8	7.78E-04
0.4	8.89E-04
0.0	1.0E-03

The cracking strains in Table 3.3 above were obtained by subtracting the elastic strain from the total strain (equation 3.7).

$$\varepsilon^{cr} = \varepsilon_t - \frac{\sigma_t}{E_0} \tag{3.7}$$

Additionally, the total strain of 0.001 when stress reduces to zero was adopted, as already mentioned (Table 3.3).

Lastly, the stiffness degradation in tension was accounted for in the material behaviour in ABAQUS through the tensile damage variables (Table 3.4) which were calculated using

equation 3.8. The data for the tensile damage was provided in terms of the tensile damage parameter and cracking strain in ABAQUS (refer to Table 3.4).

$$D_t = 1 - \frac{\sigma_t}{f_t} \tag{3.8}$$

where σ_t is the stress on the descending portion of the stress strain curve, f_t is the peak compressive stress and D_t is the tensile scalar degradation variable.

Table 3.4: Concrete tension damage input used in the study

Yield Stress [MPa]	Cracking Strain
0.00E+00	0.0E+00
1.11E-01	1.11E-04
2.23E-01	2.22E-04
3.34E-01	3.33E-04
4.43E-01	4.44E-04
5.54E-01	5.55E-04
6.66E-01	6.67E-04
7.77E-01	7.78E-04
8.89E-01	8.89E-04

The input data from Table 3.2 to Table 3.4 describe the uniaxial compressive and tensile behaviour of concrete. However, as has been alluded to earlier, concrete structures in most cases (if not all cases) are subjected to multi axial stress states in service. Thus to complete the definition of the CDP model by incorporating multi axial stress state, the parameters in Table 3.5 where used. These parameters define the plasticity of concrete. As was observed from Mundeli & Moyo (2014), five parameters govern the behaviour of concrete under the multiaxial stress state and these are summarised in Table 3.5.

The above discussed properties were assigned to the Hydropower plant model.

Table 3.5: Plasticity parameters for concrete used in the study

Parameter	Cracking Strain
Dilation angle (ψ)	30°
Eccentricity (ϵ)	0.1
Ratio of initial yield stress to uniaxial compressive stress (f_{b0}/f_{c0})	1.16
Ratio of the second stress invariant on the tensile meridian to that of compressive meridian (K)	0.67
Viscosity parameter (μ)	0.01

3.5 Implementation of Saouma's ASR Constitutive model in ABAQUS

The ASR constitutive model used in this study is a phenomenological model which was proposed by Saouma (2014). The major premises of the model include the assumption of volumetric expansion of the gel and the redistribution of stress on the basis of weights related to the stress tensor so as to induce anisotropy. Saouma's (2014) proposed model (described in equation 3.9) combines (i) the kinetics of the chemical reaction and diffusion processes with (ii) the mechanics of fracture which affects volume expansion and causes loss of strength. The combining of these two afore mentioned aspects results in the interdependency of the mechanical and chemical components in the proposed ASR constitutive model through the kinetics of the reaction. Consequently, the proposed model can also be classified as a thermo-chemo-mechanical model (Saouma & Perotti, 2006). Equation 3.9 shows the general equation for the incremental free volumetric AAR strain:

$$\dot{\epsilon}_V^{AAR}(t,T) = \underbrace{\Gamma_t(f_t'|w_c,\sigma_I|COD_{max})\Gamma_c(\overline{\sigma},f_c')}_{\text{Retardation}}\ \underbrace{g(h)}_{\text{Humidity}}\ \underbrace{\dot{\xi}(t,T)}_{\text{kinetics}}\ \underbrace{\epsilon(\infty)}_{\text{AAR Strain}} \tag{3.9}$$

Kinetics:

The kinetics of the chemical reaction and diffusion process in the proposed model where largely inspired by the research conducted by Larive (1998). From his research, Larive (1998) proposed a thermodynamically based model (equation 3.10) that governs the concrete expansion.

$$\xi(t,T)=\frac{1-e^{-\frac{t}{\tau_c(T)}}}{1+e^{-\frac{(t-\tau_l(T))}{\tau_c(T)}}} \qquad (3.10)$$

where t is time, T is the temperature in degrees Kelvin, τ_c is the characteristic time and τ_l, the latency time (Saouma & Perotti, 2006).

As can be seen in equation 3.10, Larive's (1998)'s proposed model (equation 3.10) is distinctly characterised by the two parameters: (i) the latency time (τ_l) and (ii) the characteristic time (τ_c). These two parameters define the normalised expansion curve (Figure 3.10) derived from equation 3.10.

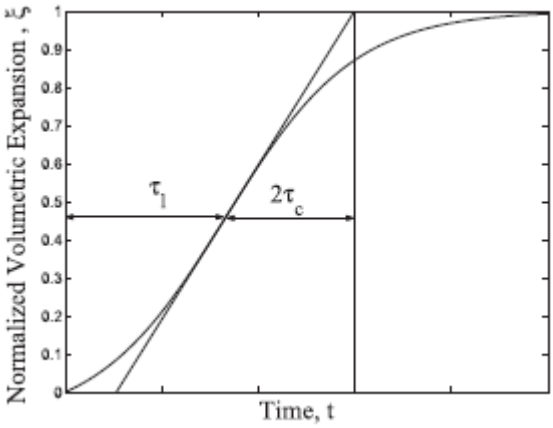

Figure 3.10: Normalised Expansion curve used (Saouma, 2014)

In this study, the following values were used for the aforementioned parameters:

$$\tau_c = 2500; \qquad \tau_l = 10\,000$$

These values (τ_c and τ_l above) were estimated from literature, as no experimental determination of these parameters for the Nalubaale Hydropower Plant have not been conducted. Consequently, these values need to be calibrated.

Retardation:

The mechanics of fracture which affects the volume of expansion, is accounted for in Saouma's proposed model through the retardation term in equation 3.9. This retardation term accounts for hydrostatic compressive stress (triaxial compressive stress) and the presence of cracks. As was alluded to in section 2.1 of this report, ASR related expansion and stress distribution are sensitive to confining stresses. Additionally, it is now generally accepted that at a compressive stress of about 8 MPa, expansion in the corresponding direction is entirely prevented or limited (US Department of Transport, 2012). For example, at the base of many dams the resulting expansion has been observed to be relatively less compared to the whole structure because under tri-axial compressive confinement, ASR related expansion is severely constrained (Saouma, 2014).

The retardation effect due to the hydrostatic compressive stress was accounted for in the model under discussion by altering the latency time (τ_l) as described in equation 3.11:

$$\tau_l(T, T_0, I_\sigma, f_c') = f(I_\sigma, f_c')\tau_l(T_0)e^{\left[U_l(\frac{1}{T}-\frac{1}{T_0})\right]} \tag{3.11}$$

where:

$$f(I_\sigma, f_c') = \begin{cases} 1 & if\ I_\sigma \geq 0 \\ 1 + \alpha\frac{I_\sigma}{3f_c'} & if\ I_\sigma < 0 \end{cases} \qquad I_\sigma = \left(\frac{1}{3}(\sigma_I + \sigma_{II} + \sigma_{III}\right) \tag{3.12}$$

and I_σ is the first invariant of the stress tensor whilst f_c' is the compressive strength. Based on some analysis of the work done by Multon (2004): α was determined to be $^4/_3$ (Saouma, 2014).

It is also worth noting that the stress dependency of the kinetic parameter τ_l through I_σ makes the constitutive model truly coupled between the chemical and mechanical phases (Saouma & Perotti, 2004).

On the other hand, the presence of cracks in concrete suffering from AAR is somewhat beneficial, as these can relieve the gel-induced stresses by providing space that is fillable by the expanding gel. Ultimately, this may result in the reduction of the final volumetric expansion. In the constitutive model under discussion, the effect of tensile cracking was accounted for in

equation 3.9 through $\Gamma_t(f_t'|w_c, \sigma_I|COD_{max})$ in which a hyperbolic decay with a non-zero residual value was adopted (Figure 3.11),

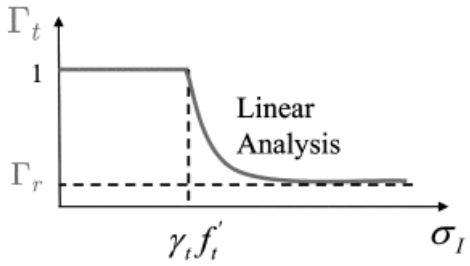

Figure 3.11: Graphical representation of normalised retardation parameters of Γ_t (Saouma & Perotti, 2004)

And is mathematically described as follows (equation 3.13):

$$\Gamma_t = \begin{cases} Linear\ elastic \begin{cases} 1 & if\ \ \sigma_I \leq \gamma_t f_t' \\ \Gamma_r + (1 - \Gamma_r)\gamma_t \frac{f_t'}{\sigma_I} & if\ \ \gamma_t f_t' < \sigma_I \end{cases} \\ Smeared\ crack \begin{cases} 1 & if\ \ COD_{max} \leq \gamma_t w_c \\ \Gamma_r + (1 - \Gamma_r)\gamma_t \frac{w_c}{COD_{max}} & if\ \ \gamma_t w_c < COD_{max} \end{cases} \end{cases} \quad (3.13)$$

where γ_t is the fraction of tensile strength beyond which gel is absorbed by the crack and Γ_r is a residual AAR retention factor for AAR under tension. For a linear elastic model, f_t' is the tensile strength and σ_I the maximum principal tensile stress. Whilst for a smeared crack model, COD_{max} would be the maximum crack opening displacement at the current Gauss point and w_c the maximum crack opening displacement on the tensile softening curve.

In addition to the already cited reason for retardation due to hydrostatic compressive stresses, retardation can also be due to gel absorption by micro-cracks induced by compressive stress. This retardation has been accounted for in the constitutive model through the term,$\Gamma_c(\bar{\sigma}, f_c')$, which is graphically represented in Figure 3.12:

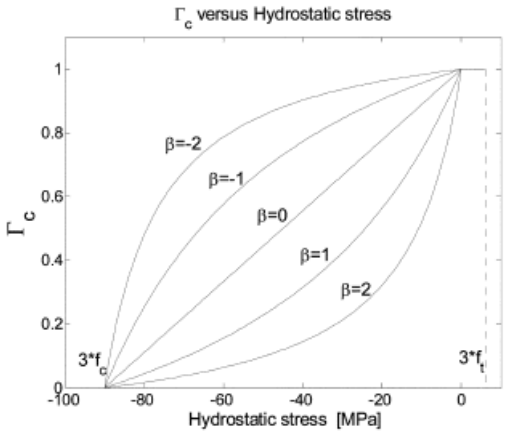

Figure 3.12: Graphical representation of normalised retardation parameters of Γ_c (Saouma & Perotti, 2004)

and mathematically described as follows:

$$\Gamma_c = \begin{cases} 1 & if \quad \bar{\sigma} \leq 0 \quad tension \\ 1 - \frac{e^{\beta\bar{\sigma}}}{1+(e^{\beta}-1)\bar{\sigma}} & if \quad \bar{\sigma} > 0 \quad compression \end{cases} \tag{3.14}$$

$$\bar{\sigma} = \frac{\sigma_I + \sigma_{II} + \sigma_{III}}{3f_c'} \tag{3.15}$$

AAR strain:

Another major proposition of the proposed model in relation to the mechanics of fracture which affects volume of expansion is that the volumetric AAR strain must be redistributed to the three principal directions according to their propensity to expand on the basis of weights which are a function of the respective stresses along the principal direction (i.e. stress state). These weights can either be based on the studies by Larive or in some cases they can be based on "simple engineering common sense" due to lack of sufficient experimental data (Saouma, 2014). Thus, the volumetric strain at a Gauss point and at time t will be given by equation 3.16, with the individual strains for the second-order engineering tensor for strain (refer to Saouma (2014)) obtained through equation 3.17.

$$\epsilon_V^{AAR}(t,x,y,z) = \xi(t,x,y,z)\epsilon(\infty) \tag{3.16}$$

where $\epsilon(\infty)$ is the free expansion assumed to be volumetric and uniform.

$$\epsilon_i^{AAR}(t,x,y,z) = W_i\dot{\xi}(t,x,y,z)\epsilon(\infty) \quad (3.17)$$

Consequently, the proposed model will result in anisotropic AAR expansion even when not expressed in tensor form because the anisotropy stems from the various weights assigned to each of the three principal directions.

Deterioration the elastic modulus and tensile strength:

The mechanics of fracture that causes loss of strength are accounted for in the model through the deterioration the elastic modulus and tensile strength. From most literature, there is little evidence of significant decrease in compressive strength due to ASR (Saouma, 2014). Thus, the deterioration of the elastic modulus and tensile strength was accounted for in the model using time-dependent nonlinear models graphically shown in Figure 3.13 and mathematically described using equation 3.18 and 3.19:

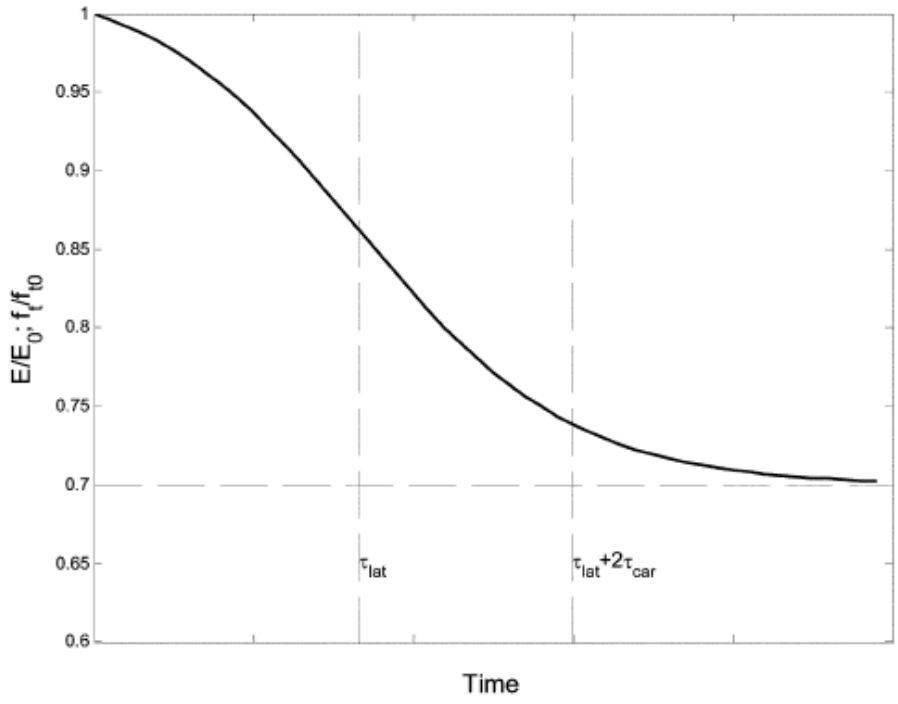

Figure 3.13: Degradation of E and f_t' (Saouma & Perotti, 2006)

$$E(t,E) = E_0[1-(1-\beta_E)\xi(t,T)] \quad (3.18)$$

$$f_t'(t,T) = f_{t,0}'\left[1-\left(1-\beta_f\right)\xi(t,T)\right] \quad (3.19)$$

Humidity:

As already noted in section 2.1 of this report, moisture availability is one of the requirements for deleterious ASR to occur and thus affects the progression of the reaction. Consequently, in the proposed ASR constitutive model used in this study, humidity related effects on the reaction are accounted for using a reduction function (equation 3.20).

$$0 \leq g(h) \leq \frac{\epsilon(t=\infty,RH=h)}{\epsilon(t=\infty,RH=1)} \quad (3.20)$$

where, *g(h)* (equation 3.21) is a function in terms of the relative humidity (*h*) which results in a reduction of the maximum expansion as at lower RH values.

$$g(h) = ae^{b.h} \quad (3.21)$$

with a and b as constants have values of 0:0002917 and 8.156 respectively (Saouma, 2014).

Generally, it is accepted that an RH of at least 0.8 is required for ASR to occur (Saouma, 2014). Moreover, a separate analysis should ideally be conducted in order to determine the spatial and temporal distribution of RH inside a structure (i.e. RH(*t*,*x*,*y*,*z*)). For dams however, the RH can be reasonably assumed to lie between 90-95% throughout the dam structure. Consequently, for dam structures, g(h) can be assumed to be 1 inside a dam for all temperatures (Saouma & Perotti, 2006).

Lastly, the ASR constitutive model proposed by Saouma (2014) is not in-built into the ABAQUS analysis software package. However, ABAQUS allows for any kind of analysis provided one can write an input script (subroutine) for whatever analysis is needed to be carried out. Consequently, in order for Saouma's (2014) constitutive model to be implemented in ABAQUS, an already developed subroutine (developed by Rodriguez et al (2011)) was used as the writing of the subroutine did not fall part of this research's scope. The subroutine is was written in INTELFOTRAN. The first step in implementing the model was to check that the provided subroutine works well (validate it against expected behaviour). The validation of the

subroutine was undertaken by Mapulanga & Moyo (2015). From their study, they concluded that there was good correlation between the model, theory, experimental and observational data in relation to loading conditions and restraints (Mapulanga & Moyo, 2015). Following from this research, the analysis was run on a single unit of the hydropower plant and then on the whole hydropower plant (10 units).

(It should be noted that to be able to carry out this analysis, ABAQUS and INTELFOTRAN had to be linked together first and the model had to be run as an input file from ABAQUS, (refer to the Appendix an example input file used in this study)).

3.6 Boundary Conditions

As already noted, ASR related expansion and stress distributions are sensitive to any form of restraint (Saouma, 2014). Consequently defining the correct boundary conditions (fixities) in the analysing of the hydropower plant was very important. The analysis was initially carried out on the single unit model before the whole Hydropower plant was analysed. Consequently, different boundary conditions were used for the two developed models (refer to Figure 3.12 and Figure 3.13).

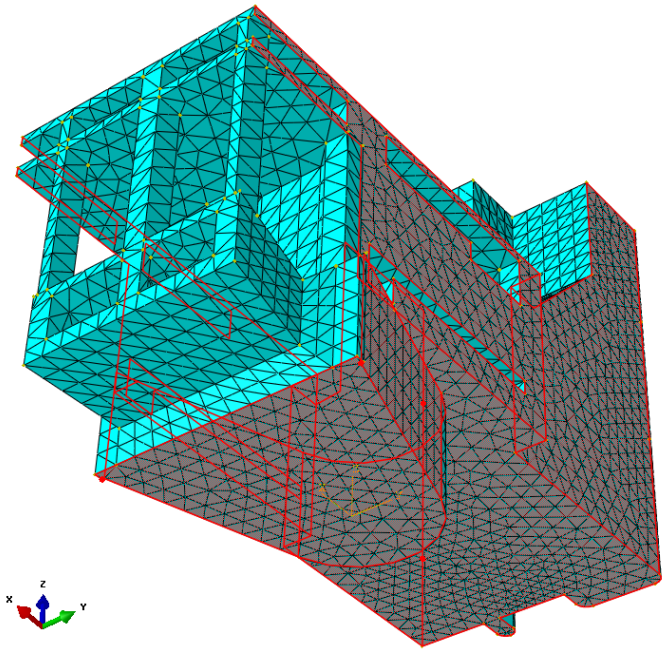

Figure 3.12: An illustration of the boundary conditions used in the analysis of a single dam unit

As can be seen in Figure 3.12, for the analysis of the single unit model, all the sides and bottom of the one unit model where fixed. This is because plane stress state (in the x-z plane) analysis was assumed since the dimension of the hydropower plant in the y – direction is significantly larger than the corresponding x – and/or z – directional dimensions. Consequently, in the analysis of the single unit, not much displacement was anticipated in the y- direction as compared to the other two directional axis due to the restraining effect that the length of the plant in the y- direction posed.

On the other hand, for the complete Hydropower plant model, the boundary conditions where applied so as to try and idealise as close as possible, the restraints the hydropower plant experiences due to its fixities based on the analysis of the plant's drawings. Figure 3.13 illustrates the boundary condition used in the analysis of the complete Hydropower Plant.

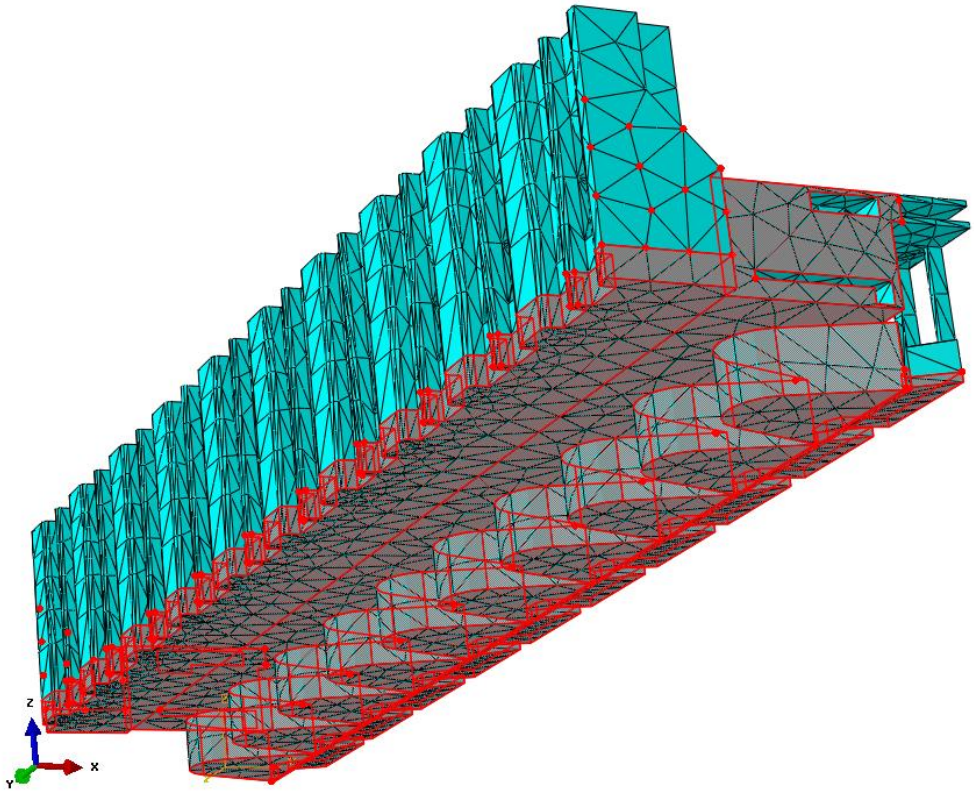

Figure 3.13: An illustration of the boundary conditions used in the analysis of the Hydropower plant

3.7 Chapter Summary

In summary, this chapter covers the steps followed in successfully developing a numerical model for Nalubaale Hydropower Plant. The plant is located in Uganda and has been diagnosed with degrading ASR that has resulted in severe cracking and dysfunction of the hydropower plant. Consequently, a numerical model of the plant was developed for analysis in ABAQUS. The plant's geometry was developed using SOLIDWORKS then exported into ABAQUS. An ASR constitutive model proposed by Saouma (2014) was used to simulate the effects of ASR on the hydropower plant and the Concrete Damage Plasticity constitutive material model in ABAQUS implemented to simulate the material behaviour of concrete. Two models which include (i) a single unit and (ii) the complete hydropower plant were developed for analysis.

4 RESULTS AND DISCUSSION

4.1 Introduction

This chapter provides an analysis of the results obtained from (i) the single dam-generator unit (Figure 4.1) and (ii) the complete hydropower plant (i.e. 10 generator units) (Figure 4.6) numerical models. Further, the results and discussions of both models and any supporting site observations were integrated together so as to provide a good understanding of the model(s) results in relation to site observations. Since the constitutive ASR model has already been validated in a separate study undertaken by Mapulanga & Moyo (2015), the structural behaviour of the hydropower plant will be confirmed first. Secondly, results relating to understanding the model will be discussed, after which a short discussion on the potential use of the information derived from the result follows. This chapter will end with a brief summary of the discussion.

4.2 Confirming the Structural Behaviour of the Numerical model (Validation)

The first step in the analysis of the developed models was to compare the structural behaviour of the finite element models (FEM) (also referred to as numerical model in this report) to the observed and expected behaviour of the hydropower plant. This analysis was achieved by comparing (i) the overall deflected shape, (ii) the generator floor cross-sectional displacement profile, and (iii) tensile damage (which is assumed to be associated with the cracking pattern) of the developed model(s) to the on-site observations and measurements.

4.2.1 Confirming the overall deflection of the model

Figure 4.1 shows the overall deflected shape of the Hydropower plant as obtained from the developed model(s). Some of the deflections at different points on the structure have been highlighted in Figure 4.1 ($\Delta_1, \dots, \Delta_5$). As was expected and similar to site observations, the developed model(s) had an overall upward movement (Δ_z) and downstream movement (Δ_x).

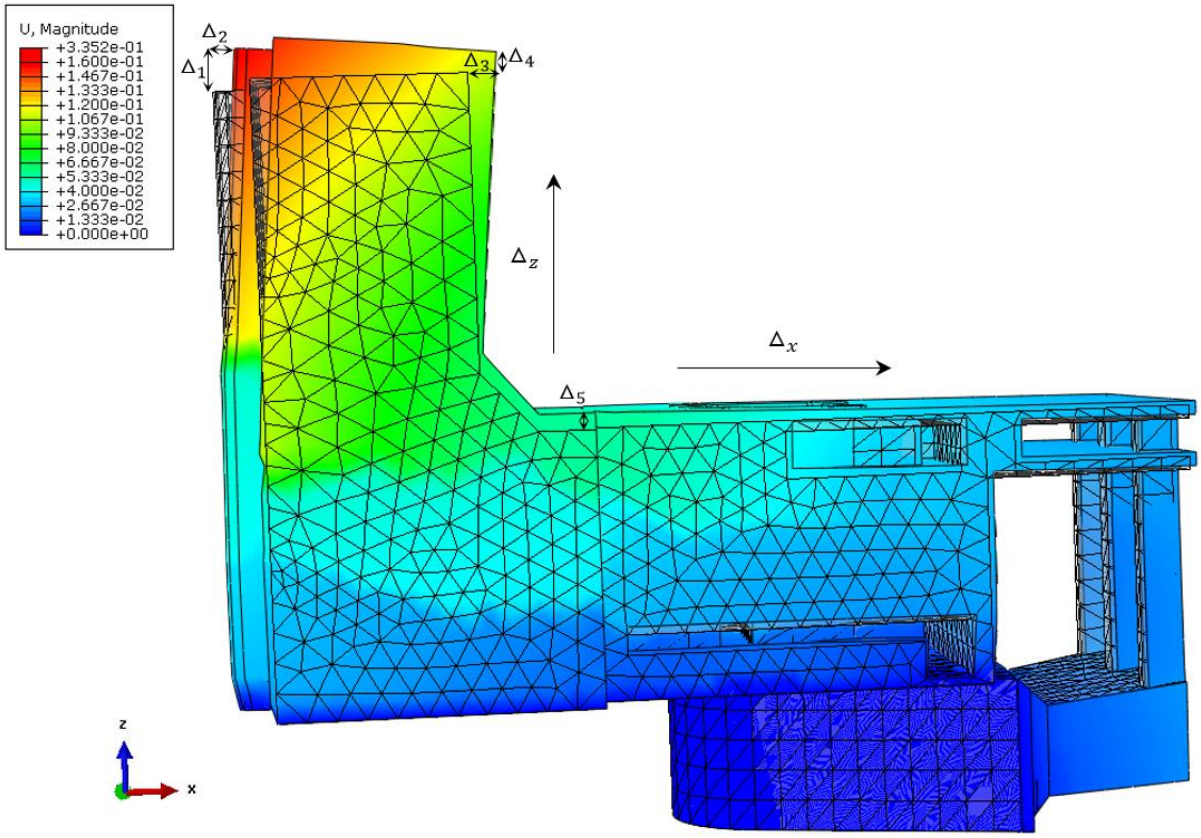

Figure 4.1: Overall deflection of Plant as obtained from the developed model

Additionally, the hydropower plant's downstream wall has been observed to rotate downstream about a hinge point (highlighted area marked O in Figure 4.2) immediately above the draft tube. This rotation resulted in the displacement profile on the downstream columns illustrated in Figure 4.3 below. However, the displacement profile along the columns in the downstream direction of the developed models did not resemble the observed displacement profile (Figure 4.3). Of the two models, the downstream column profile of the single unit hydropower plant seemed closer to the observed displacement (Figure 4.3). Further, the rotational movement that was observed on the Hydropower plant (Figure 4.2) does not clearly show from the models. These observed differences might be attributed to the difference in material properties of the concrete used in different sections of the plant (refer to Figure 4.4 below). The Stage 2 concrete is thought to be more severely affected by ASR compared to the stage 1 concrete (Figure 4.4). Yet, homogeneous concrete properties throughout the hydropower plant numerical model(s) were assumed, which clearly, was not a completely accurate assumption.

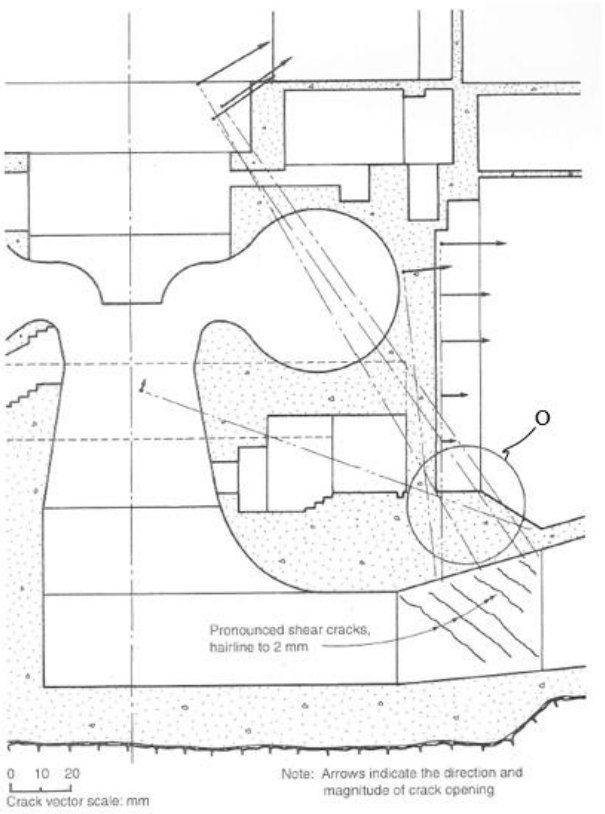

Figure 4.2: Cross-section through the power plant showing the downstream rotation and shear cracks in the draft tube side wall (Mason & Molyneux, 1998)

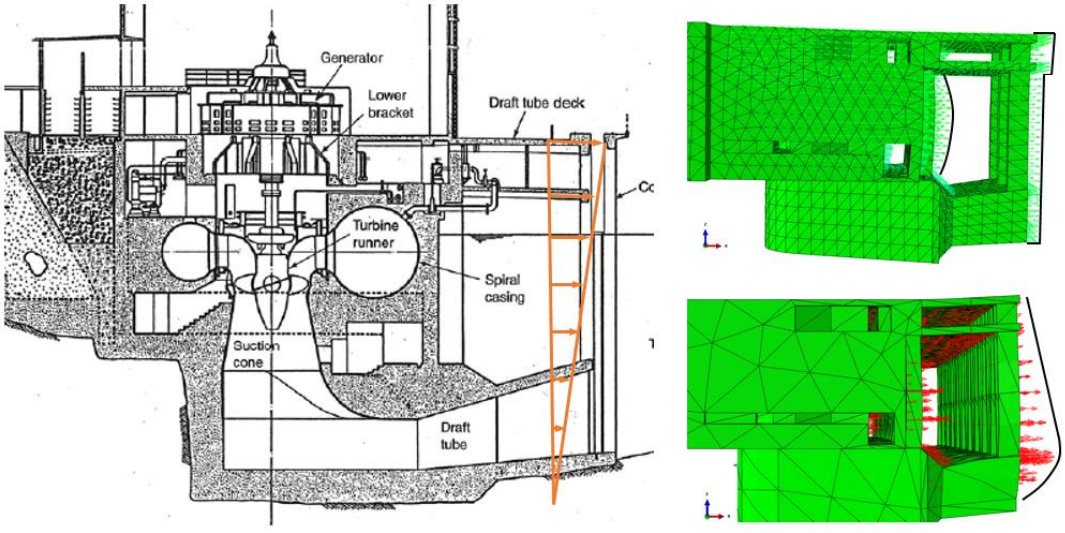

Figure 4.3: Comparison of displacement in the x – direction along the downstream end of the hydropower plant

The image on the left in Figure 4.3 above shows the downstream displacement along the downstream end correlating to the displacement as shown in Figure 4.2. Whilst the images on the right in Figure 4.3 illustrate the downstream displacements obtained from the FEM analysis. The top right image shows the displacement profile along the downstream end of the single Hydropower plant unit model and the bottom right image shows the displacement profile along the downstream end of the complete hydropower plant model.

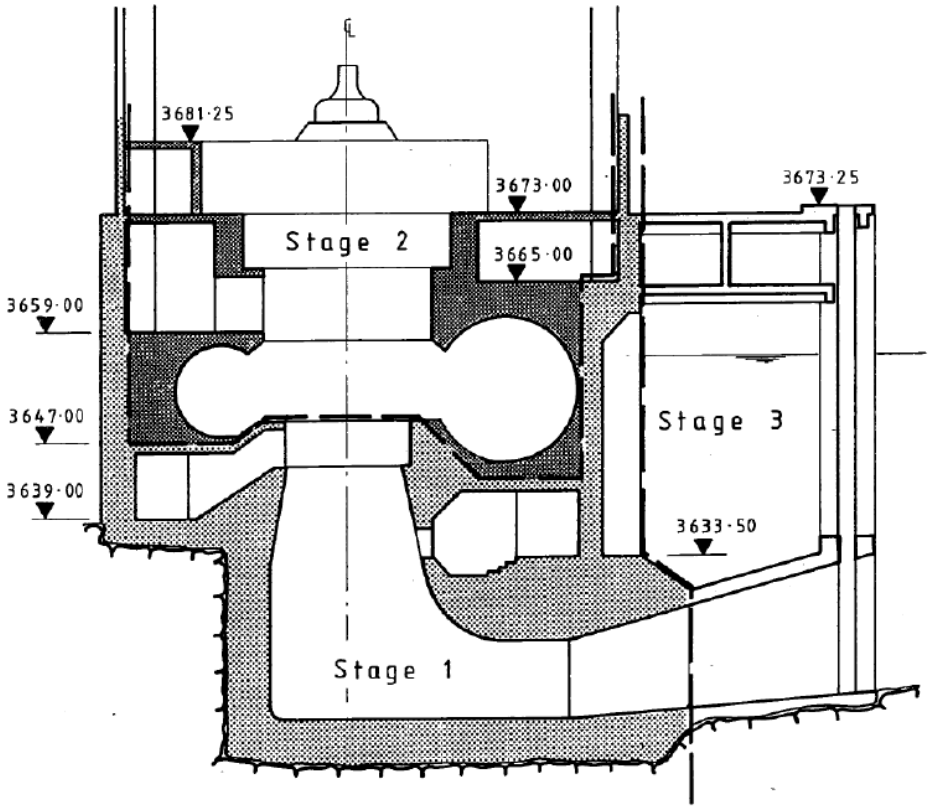

Figure 4.4: Image showing construction stages of the plant's structural component housing the generators (Mason & Molyneux, 1998)

Furthermore, Mason & Molyneux (1998) also noted that the downstream wall of the power station was heavily reinforced at its base resulting in the observed rotation pivot (Figure 4.2) being directly above the heavily reinforced wall. Since homogeneous concrete properties were assumed throughout the developed numerical model(s), differences in stiffness of different parts of the structure were not considered in the numerical modelling. This could be another reason why the downstream rotation about area O (Figure 4.2) was not observed in the numerical model analysis.

4.2.2 General displacement profile along the length of the hydropower plant measured at the centre of each generator housing set

Figure 4.5 below is a comparison of the displacement measured at the Generator Set Centre lines on site and that obtained from the developed numerical model.

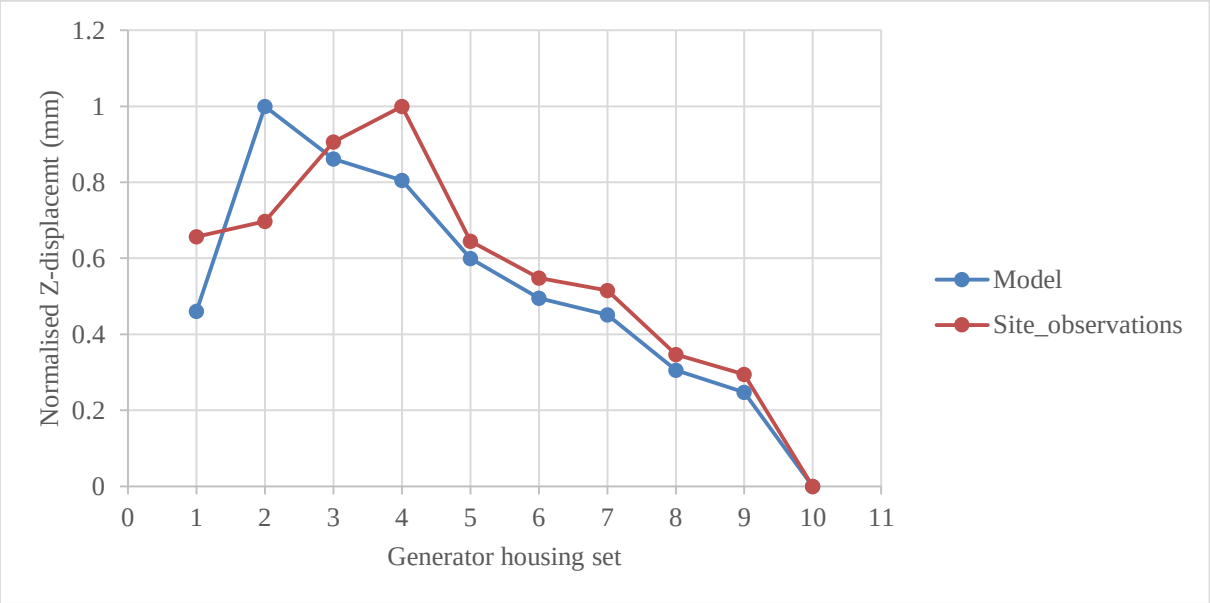

Figure 4.5: Normalised Hydropower plant floor rise at generator set centre-lines

Both graphs have strikingly similar displacement trends across the Generator housing floor apart for set 2, 3 and 4 (Figure 4.5). Moving from generator set 4 to set 2 the normalised displacement obtained from the model continued to increase whilst the site measured normalised displacement were observed to decrease (Figure 4.5). The difference in the trends observed above (Figure 4.5) as one moves from generator set 4 to set 2 might be attributed to the fact that the first three generator sets (set 1, set 2 and set 3) especially set 1 have been observed to show the least extent of damage and/or symptoms due to ASR from site investigations (Mason & Molyneux, 1998). Although the cracking patterns related to ASR was observed to be similar for most generator sets in site investigations, the cracking patterns were focused more heavily on generator sets 5 to 10. The observed difference in the intensity of cracking in different generator housing sets on site can be attributed to the use of different types of cements in the construction of the Hydropower plant. Initially, imported Rugbv cement from UK cement was used for the construction of the hydropower plant. But about midway through the construction, Toronto cement which was then locally produced in Uganda was used to

complete the construction of the plant. The latter cement proved to be rich in alkalis thus making it more susceptible ASR (Mason & Molyneux, 1998). Consequently, the disparity in the graphs shown in figure 4.5 (sets 2, 3 and 4) might be attributed to the assumption of homogeneity of the material and in the uniform application of the ASR constitutive model in the numerical analysis. As a result, the difference in reactivity of the cements used for different areas of the hydropower plant was not accounted for in the numerical analysis.

Figure 4.6 below illustrates the positions of each generator set in relation to the Hydropower Plant.

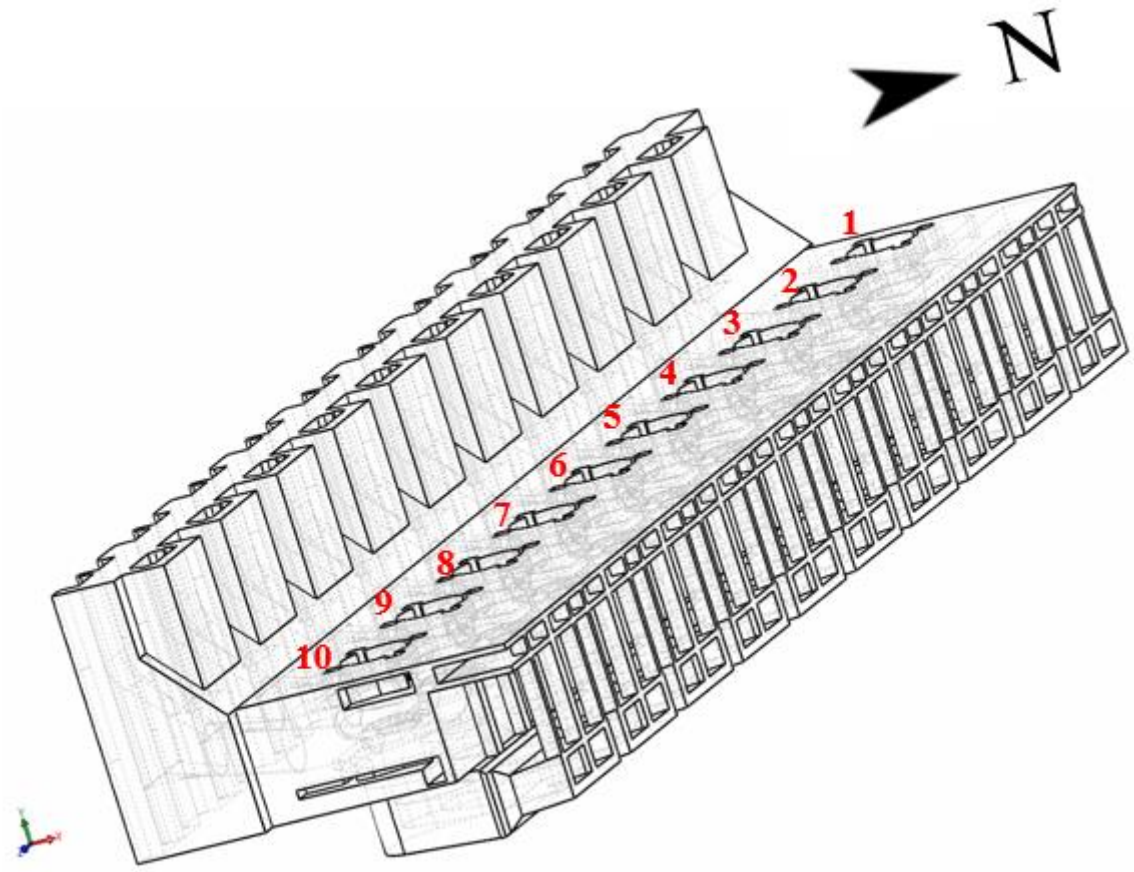

Figure 4.6: Illustration of the Generator Set Numbers as used in this research

4.2.3 Confirming the structural behaviour of the dam by comparing crack patterns

Additional to the overall displacement of the model and floor displacement, the cracking pattern observed from the model correlated well with site observations. (Figure 4. 7 shows the cracking as observed from the single generator set model.)

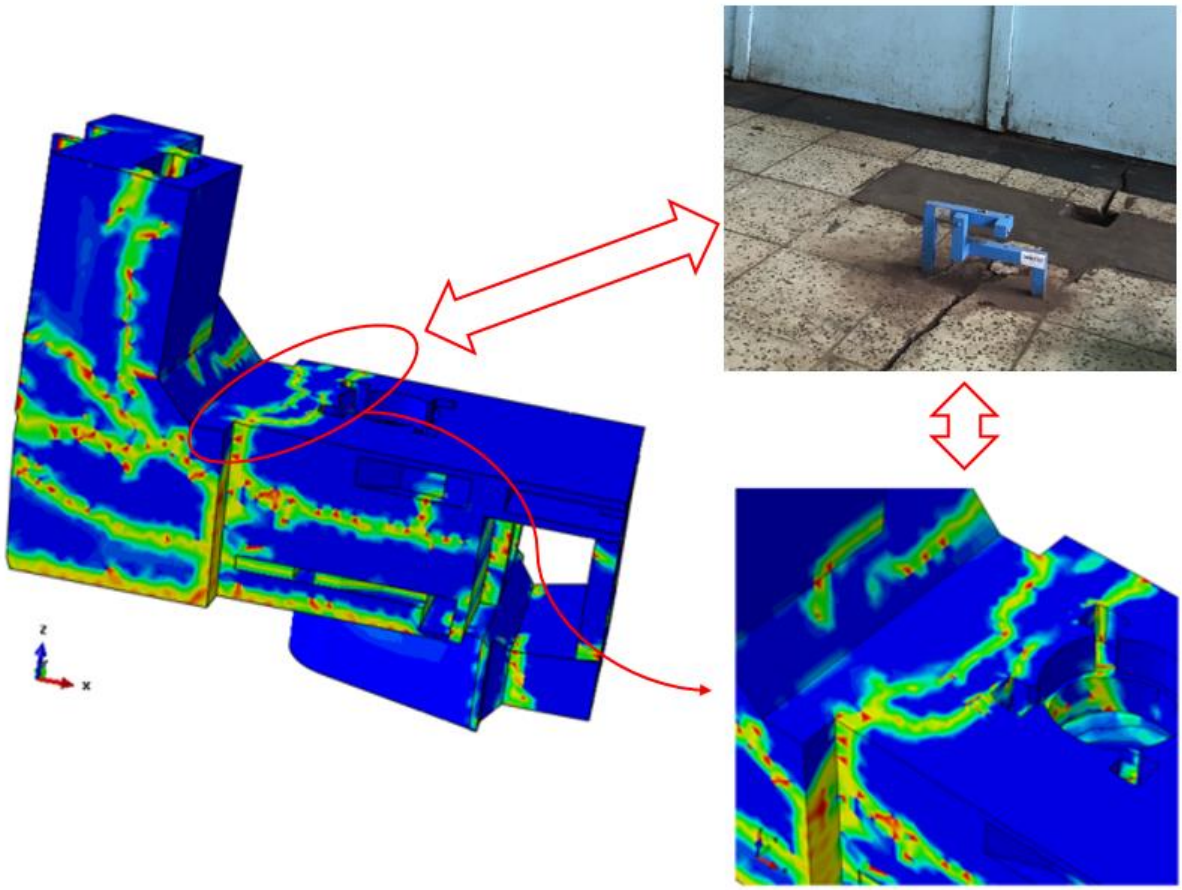

Figure 4.7: Cracking pattern observed from the numerical analysis of the single generator unit

From site investigations of the hydropower plant, similar crack patterns to those obtained in the numerical analysis were observed. For example, a longitudinal crack along the machine hall floor (Figure 4.7: top right image) was observed in the initial inspections conducted by the design engineers in 1983 and has continued to grow since. Additionally, another severe crack was observed on the underground corridor bordering the alternator block housing wall (Figure 4.8). This was also clearly observable in the numerical model analysis (see Figure 4.8)

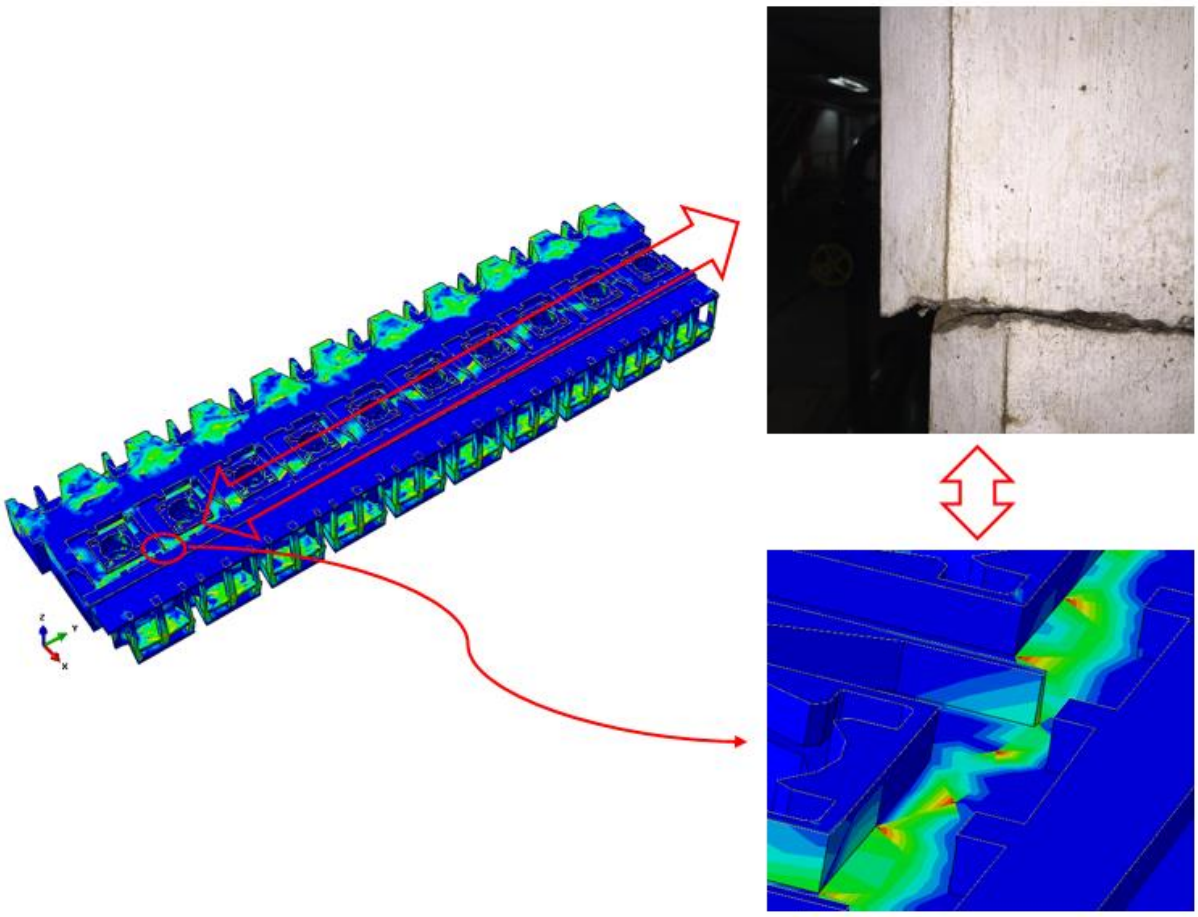

Figure 4.8: View of cracking at the alternator block cross-sectional cut of the Hydropower Plant

As can be seen in Figure 4.8 above, the image on the top right is an image taken in one of the site investigations. The two model images show the relative position of the observed crack in the Hydropower plant, thus, relating the model analysis crack pattern to the site observations.

The correlation of cracking from the numerical modelling results and the site observations, together with the validation of the overall deflected shape and floor displacement profile of both the numerical analysis and site observations serve to confirm the structural behaviour of the hydropower plant as observed from the numerical model analysis results.

4.3 Understanding the model

As already highlighted in section 1.4 of this report: the only available site measurements to be used to calibrate the model where obtained from already processed data graphs as were found in different reports related to the assessment of the plant by researchers and consultants. Additionally, (to the best of the knowledge of the author) the only measurements directly measuring displacement (vertical displacement in this case) where installed on the generator power housing floor and there was no evolution of the displacement with time for a particular point that was found. Thus, in this analysis, it was assumed that the crack width measurements could give a relatively good approximation of the evolution of displacement at a point over time. (However, further research could be done to ascertain whether this is the actual case).

4.3.1 Displacement profile obtained from crack width measurements onsite

Figure 4.9 shows the normalised crack growth evolution which was assumed to approximate

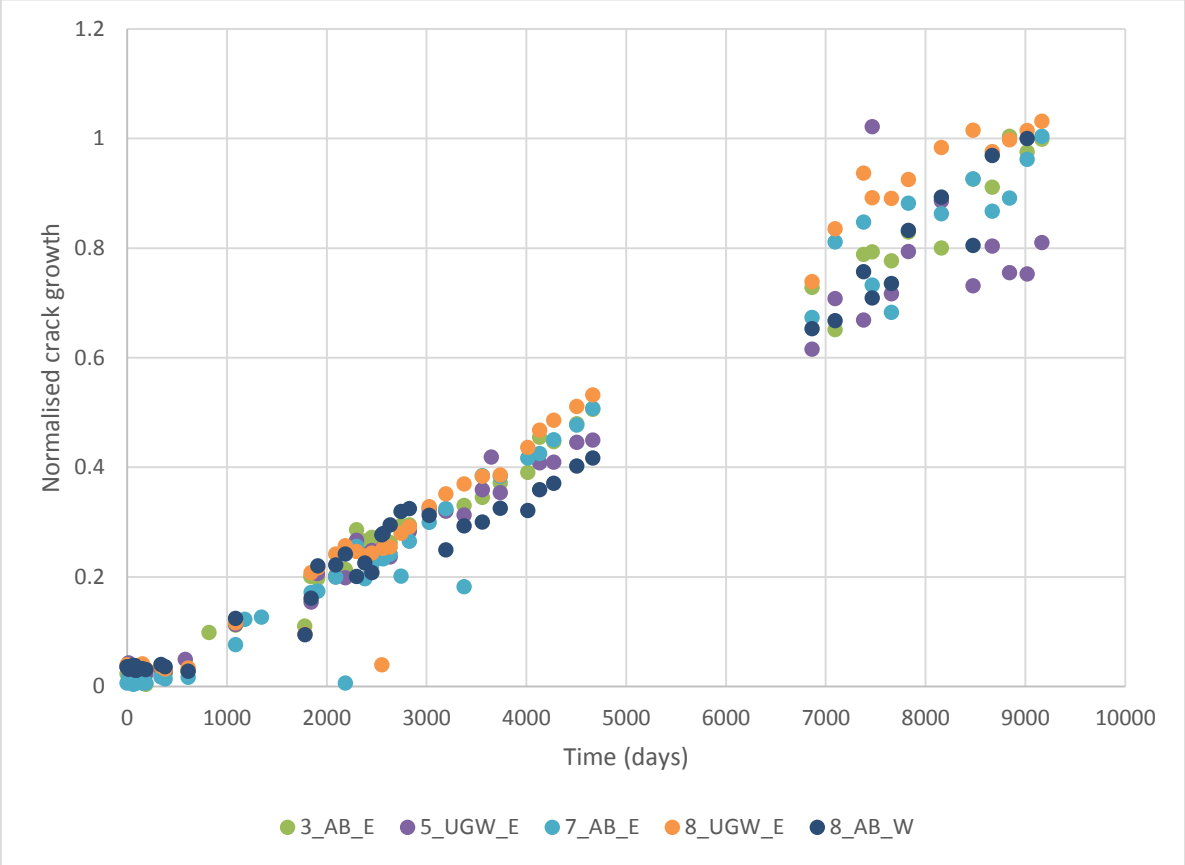

Figure 4.9: Displacement profile based on the crack width measurements onsite

the rate of expansion due to ASR. The measurements used to derive these graphs (Figure 4.9) dated from 1989 to 2015. Since crack growth evolution values were used to approximate the rate of expansion due to ASR, the influence of other loads such as the hydrostatic loads was assumed not to significantly contribute towards the crack growth as these other loads generally result in the displacement of the wall structure.

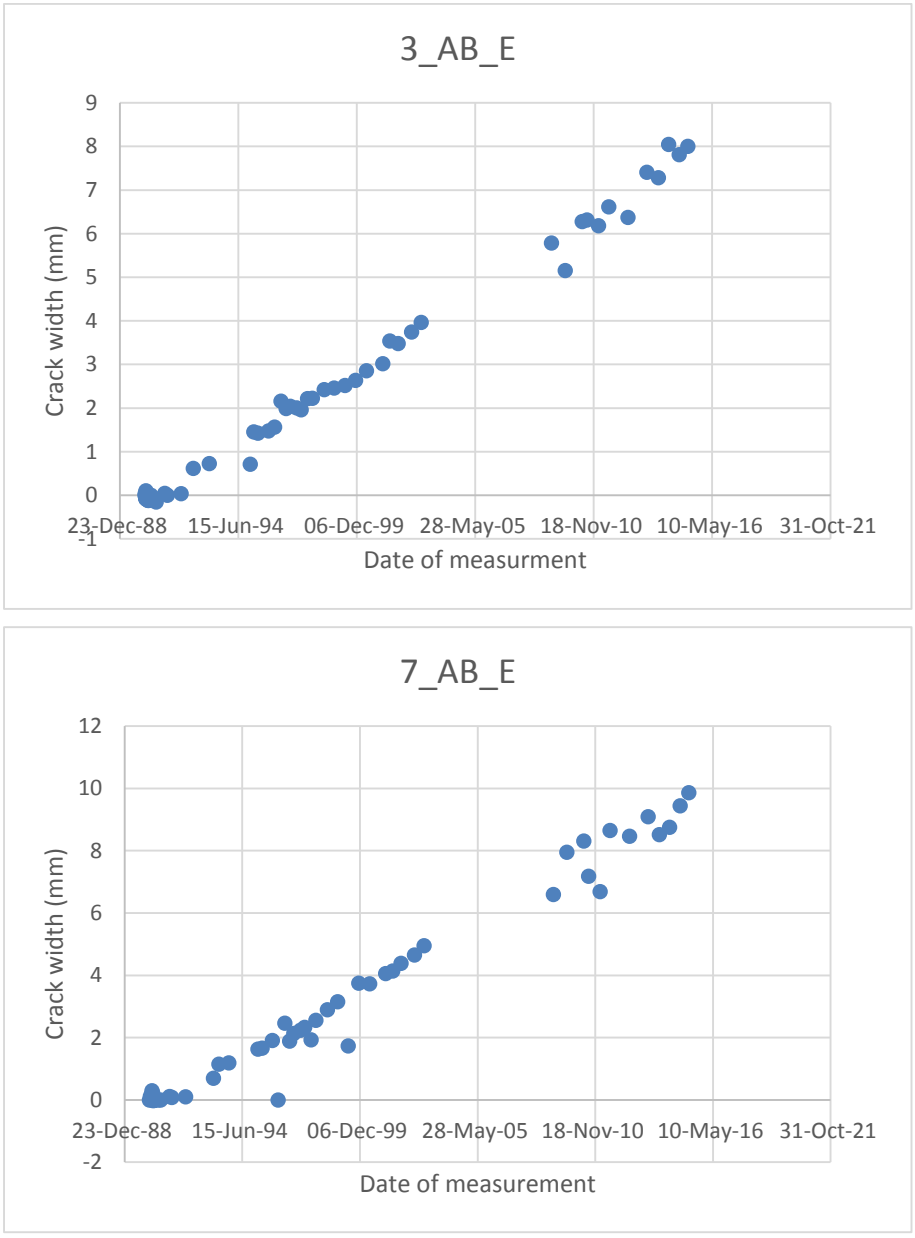

Figure 4.10: Typical Crack growth evolution as measured onsite

The displacement after 36 years (in 1990) up to 60 years (in 2015) of the dam in service where pretty much linear (Figure 4.10) with little to no signs of the displacements progression tailing down.

4.3.2 General displacement profile at similar points as the crack width measurements points on the model

Using similar site locations on the numerical model as to those in Figure 4.9 above, the displacement evolution over approximately 40 years was observed to pretty much follow the theoretical proposed reaction extent S-curve (Figure 4.11 & Figure 4.12).

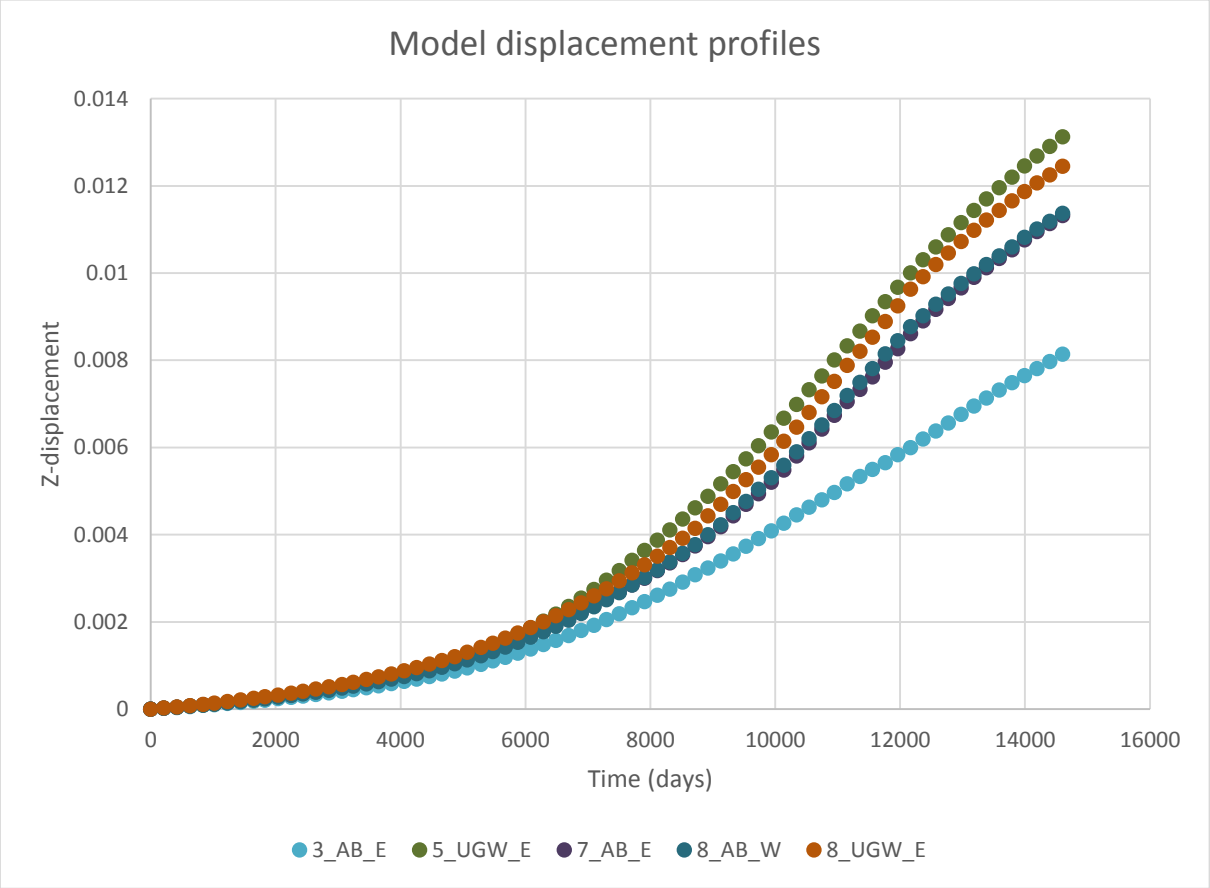

Figure 4.11: Displacement profile based of similar point locations as those in Figure 4.12

Figure 4.11 shows the scatter in the displacement graphs when put on one graph whilst Figure 4.12 shows single typical displacement profile graphs over time. The graphs in Figure 4.11 were Normalised and then plotted together with the reaction extent graph used in the model(s)

analysis (Figure 4.13). The displacement graphs and the reaction extent graph had the same trend for about 11 000 days (approximately 30 years). However, as the reaction extent graph

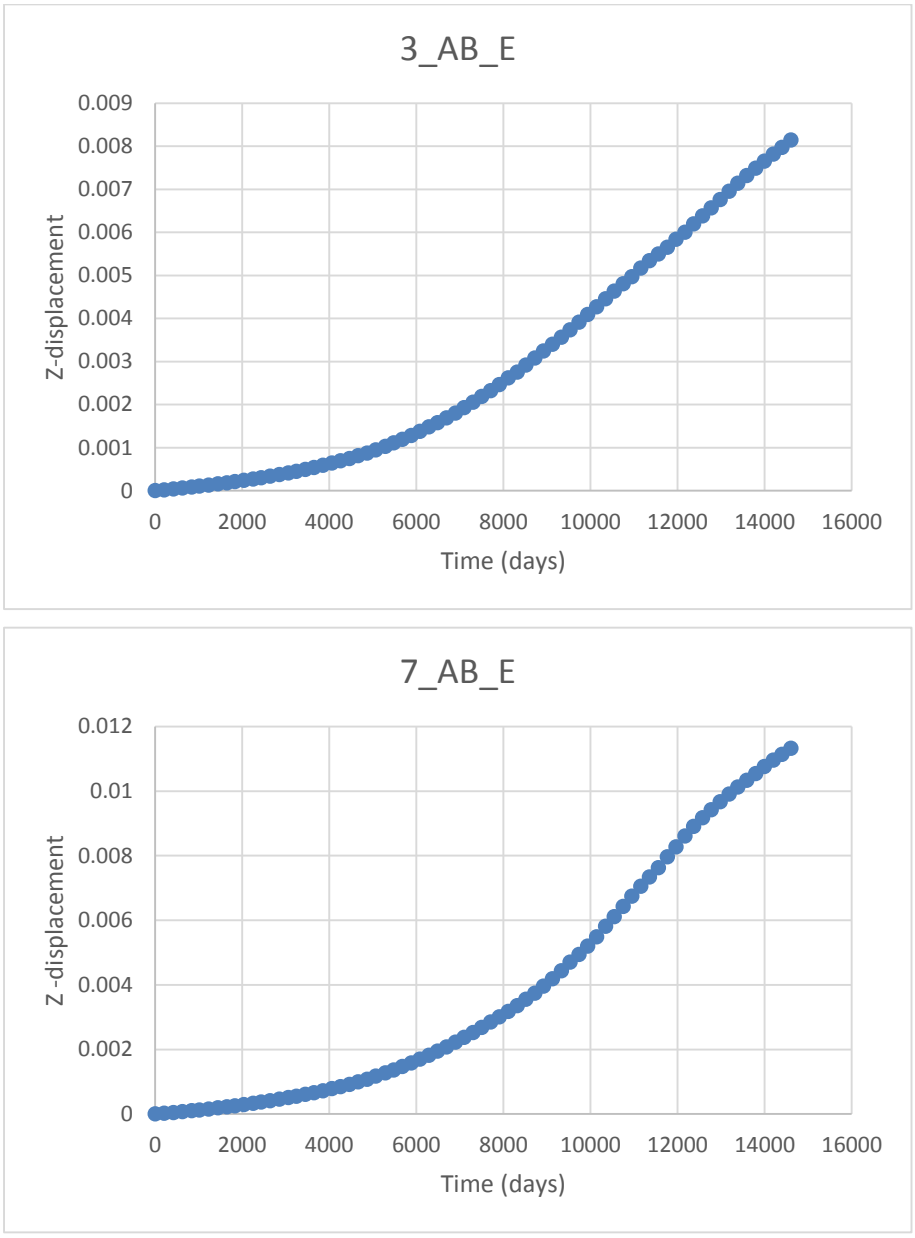

Figure 4.12: Typical Crack growth evolution from the model

tails down, the displacement graphs seem to continue somewhat linearly with a slight tailing down at the end of the graph. This finding seems to suggest that the displacement due to ASR might not necessarily follow directly the ASR reaction extent, but the displacement can continue to increase even though the reaction is tailing down.

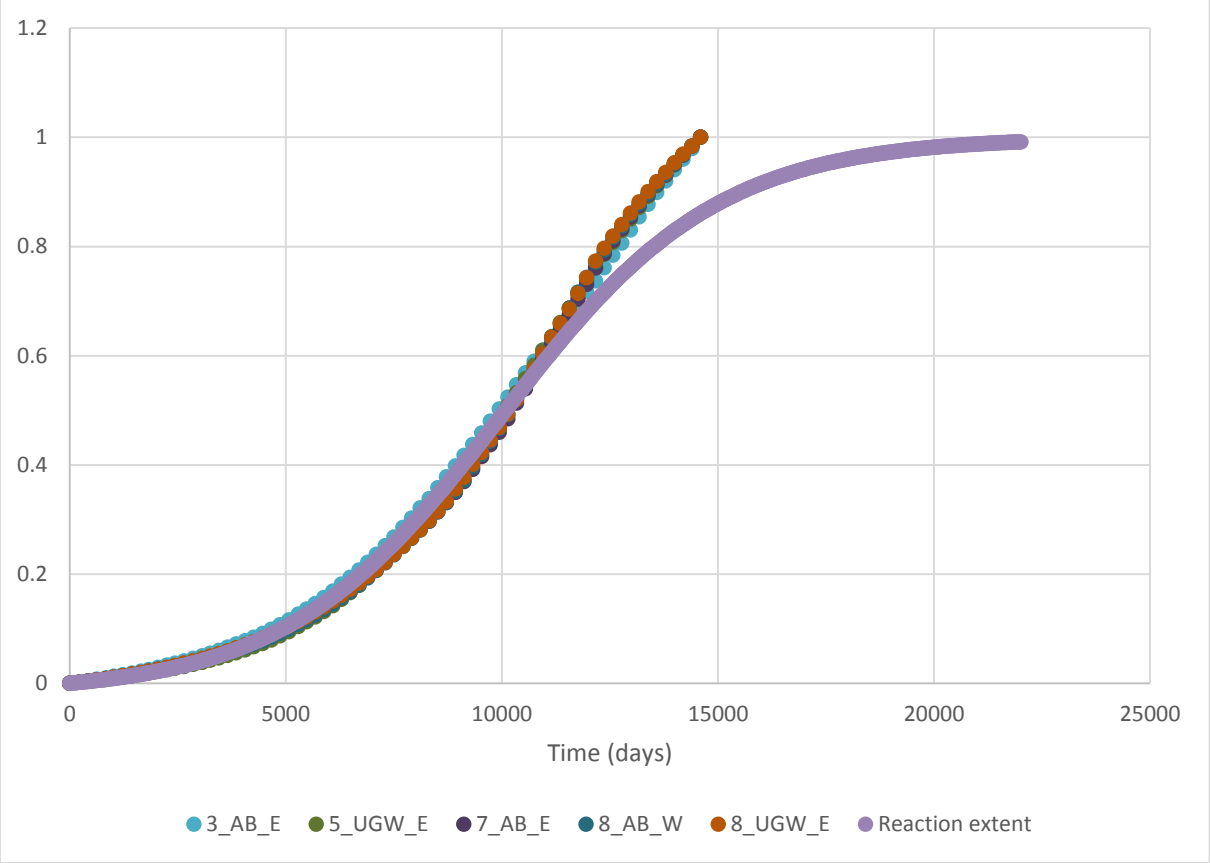

Figure 4.13: Comparison of the model displacement trend to the reaction extent trend

4.3.3 Comparison of the displacement profiles from the model(s) to those obtained from site measurements

The model analysis ran for about 40 years whilst the crack width measurements used to develop the displacement profiles shown in section 4.3.1 were recorded from about the year 1989 (about 35 years since the dam went into operation). Thus, to be able to compare the displacement profile trends from both the model and the site measurement, the graphs where normalised so they could be put in the same graph (Figure 4.14). Additionally, the displacement profile from the model and the site measurements only share about a 5 year period in common. The 5 year overlap between the numerical model results and the site measurements can be observed in Figure 4.14.

The displacement trend analysis seems to suggest that the reaction on the hydropower plant is not slowing down but continues linearly (Figure 4.14).

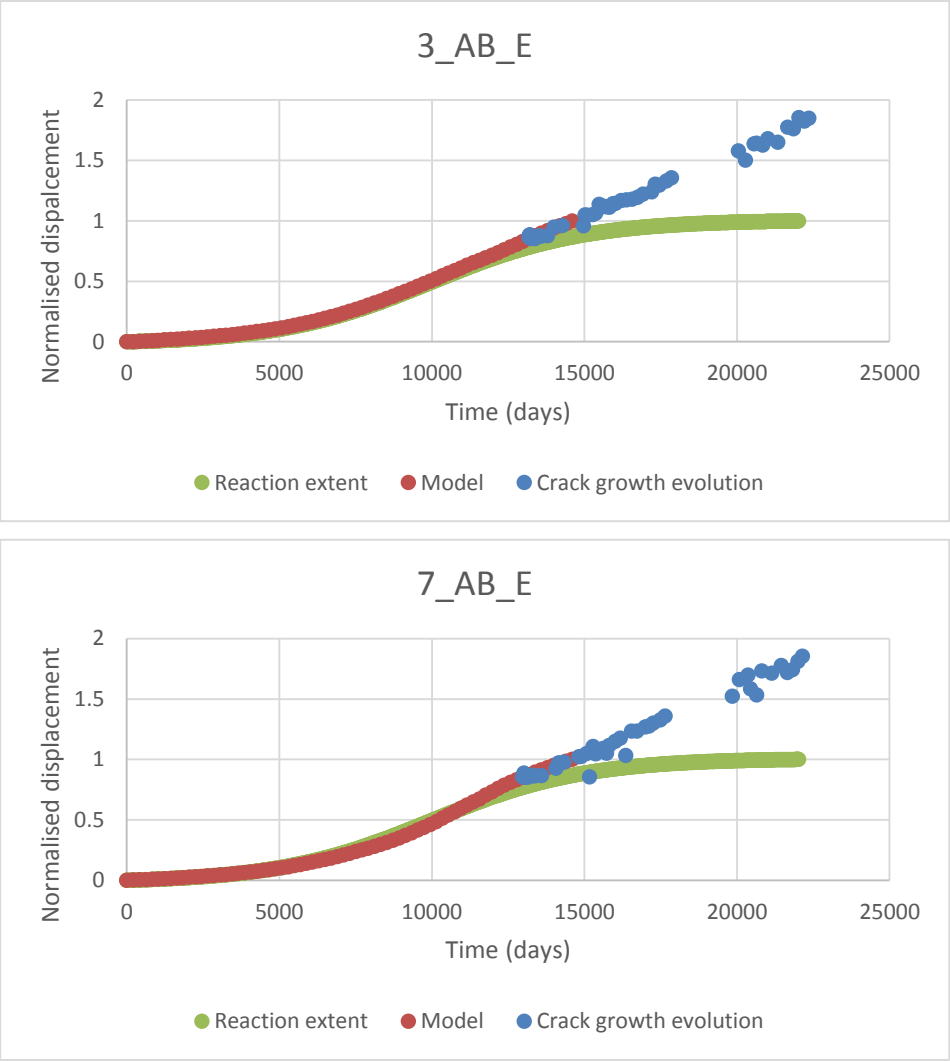

Figure 4.14: Comparison of the model displacement trend to the reaction extent trend

4.4 Further Comments and Discussion

Since the displacement profile from the model seems to be tailing down (Figure 4.13) whilst the displacements from site measurements are progressing linearly and since the latency and characteristic times used in the analysis were never calibrated, there might be a need to rerun the numerical model with updated latency and characteristic time to in order to get a more accurate representation of the observations on site from the numerical analysis. To this end both the model and site measurements were normalised together as one continuous displacement profile and a reaction extent curve fitted over the displacement profile (Figure 4.15) so as to get

estimates for the latency and characteristic times that could be used and validated in future numerical analysis of the Hydropower plant.

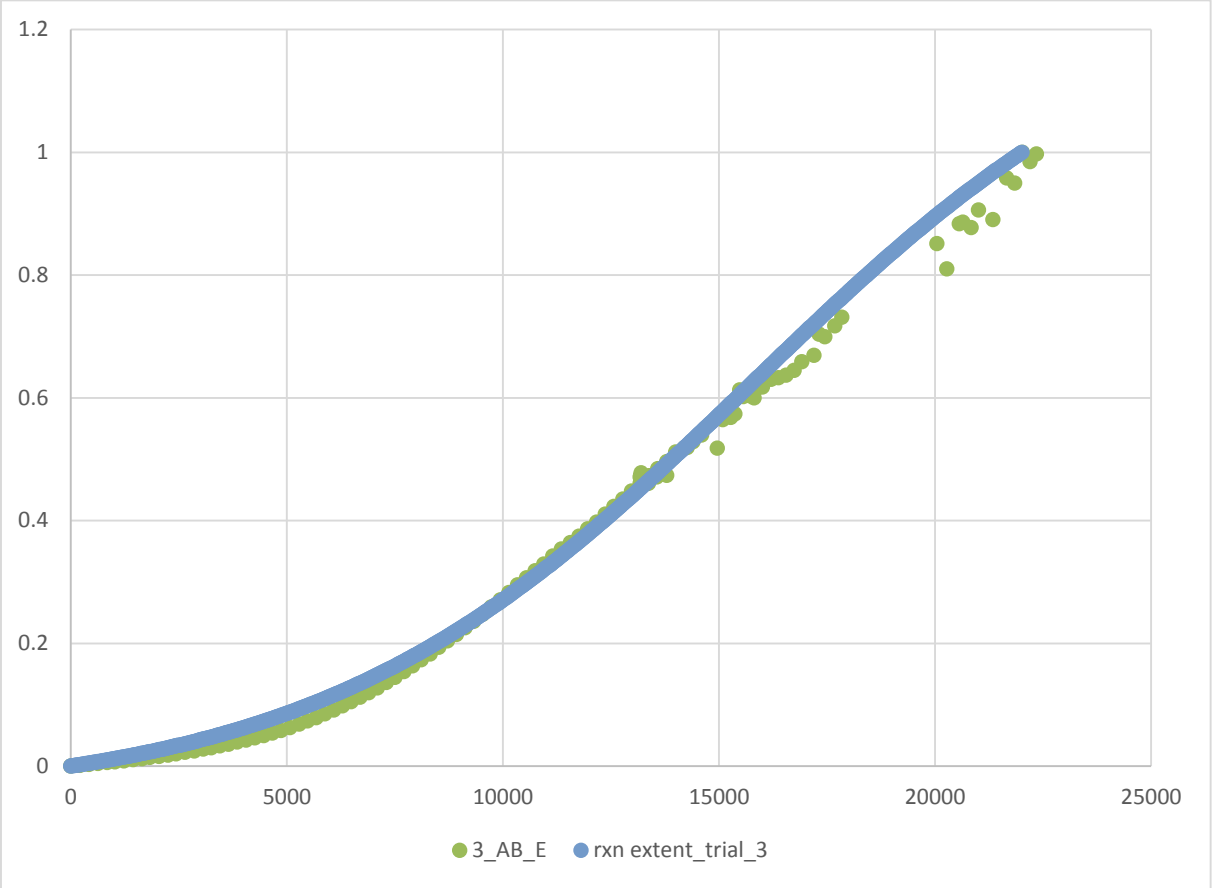

Figure 4.15: Comparison of the model displacement trend to the reaction extent trend

From the curve fitting above, τ_l = 15 750 and τ_c = 5000.

Additionally, as has been noted by many researchers, the exhaustion of ASR has been rarely observed (Giorla, 2013). This suggests that many structures (including Nalubaale Hydropower Plant) might be experiencing a linear progression of the ASR over their service life. Consequently the assessment, management and definition of the point at which these structures may be rendered unsafe might have to be carefully looked at or rethought. One way in which the assessment of these structures which exhibit a linear progression of the reaction might be undertaken is by considering two possibilities at every point of structural assessment and evaluation: (i) the reaction continues to progress linearly (worst case scenario) and/or (ii) exhaustion of the reaction is observed (Figure 4.16). Figure 4.16 illustrates these two possible prognostic proposals.

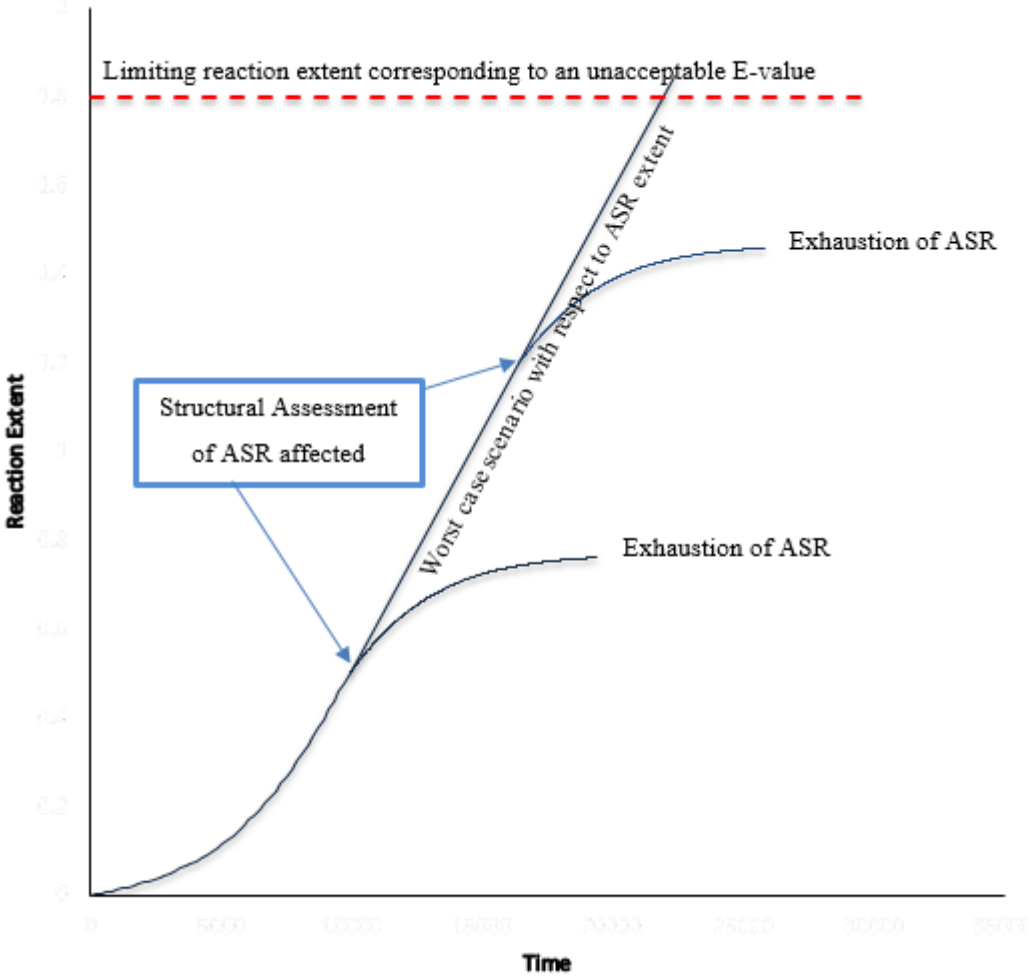

Figure 4.16: Proposed prognostic evaluation option

For the latter proposal, since some structures have been observed to show an exhaustion of the reaction, when site observations and/or numerical evaluations seem to suggest (confirm) a prognostic conclusions of the start or existence of the exhaustion process of the reaction, it can be assumed that the structure can survive failure provided the structural integrity of these structures has not been severely compromised. Thus, the aforementioned conclusion can only be reached subject to a thorough structural assessment by qualified personnel.

On the other hand, if the prognosis is the worst case scenario, one possible way of defining a limiting state or value for the design life of the structure might be through the degradation of the young's modulus (E). In Saouma's proposed model, he accounted for the degradation of E using equation 3.18 and graphically represented in Figure 4.17. As can be seen in the Figure 4.17, he assumed that the degradation varies inversely with the reaction progression (i.e. is a

function of the reaction extent). Consequently, assuming that this degradation profile holds, or if a good relationship between the reaction extent and the degradation of E for a particular structure can be obtained and validated, there exists a point where the degradation of E will reach unacceptable limits (assumedly). This point could be the limiting point which can be used to estimate an expected service life for a particular structure.

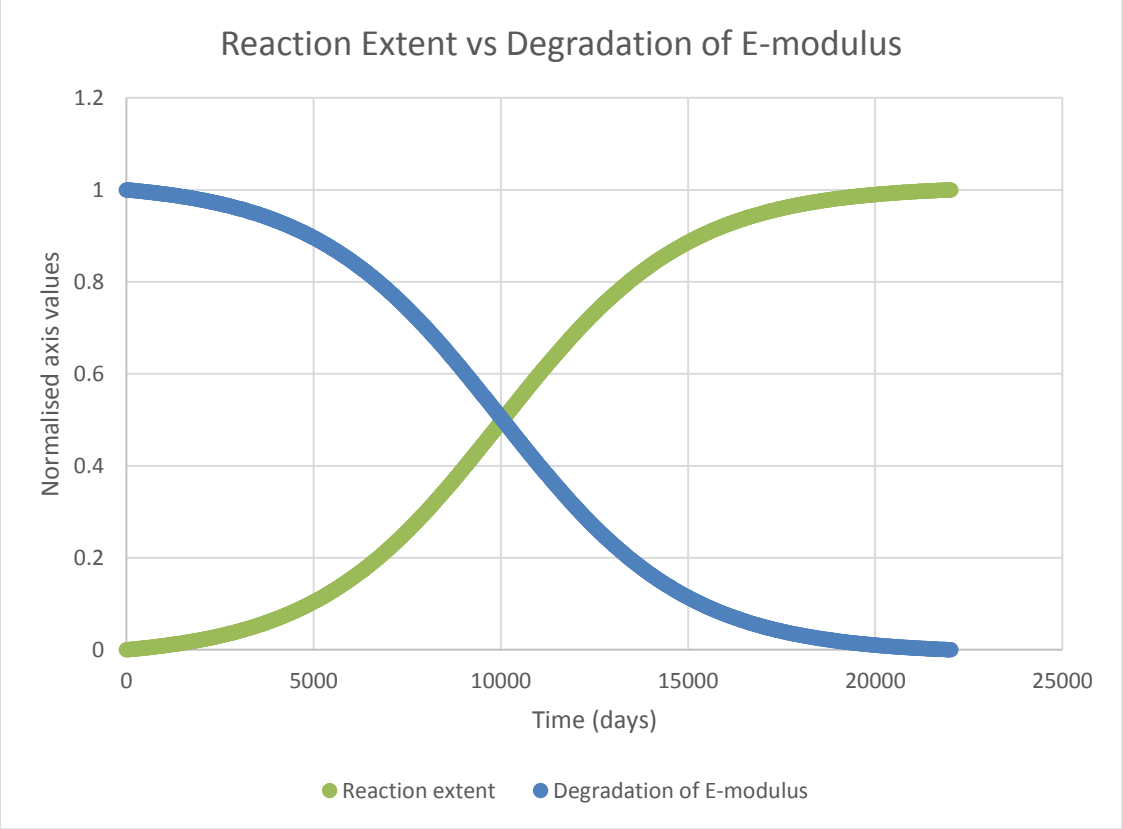

Figure 4.16: Comparison plot of the degradation the Young's modulus and the reaction extent

4.5 Chapter Summary

In summary, this chapter contains the results and discussions that carry out the objectives of this study. Initially, the developed numerical models are calibrated and validated through the consideration of the overall deflected shape of the hydropower plant, floor displacements and tensile cracking. Thereafter, a comparative study of the displacement and reaction extent profiles of both the numerical model and site observations ensues. From this study it was observed and concluded that the reaction is progressing linearly with respect to Nalubaale

hydropower station. Consequently, a prognostic approach to predict the life expectancy of the plant using the degradation of E was proposed.

5 CONCLUSIONS AND RECOMMENDATIONS

Structural degradation due to ASR of many structures worldwide has resulted in structural integrity concerns of these structures (Saouma, 2014). The objective of this study was to develop a working model that can be used in future studies to evaluate, assess and predict the structural effects of ASR on Nalubaale hydropower plant. Consequently, the objectives pertaining to this study are concluded below and future aspects to be considered going forward are provided in the recommendations section.

5.1 Conclusions

The numerical model for the Nalubaale Hydropower Plant was successfully validated and calibrated. Based on the evaluation of the results and the corresponding discussion (Section 4), the following conclusions were drawn:

(i) The overall deflected shape of the hydropower plant correlated well with site observations,

(ii) Additionally, the cross-sectional floor displacement profile from the model and the site observations correlated well with the exception of three points due to the difference in material assumptions used in numerical analysis model, which are different for the real structure,

(iii) Moreover, the cracking pattern observed from the numerical analysis results correlated well with the site investigation observations.

In addition to the difference noted in (ii) above, a downstream rotation of the plant which was observed on site could not be clearly observed in the numerical analysis due to the already mention difference in the material assumption which did not account for the differences in the extent of the reaction and stiffness throughout the hydropower plant.

5.2 Recommendations

The following recommendations are suggested for future works related to this topic:

(i) In subsequent studies, a thermal analysis of the hydropower plant should be undertaken before the implementation of the ASR constitutive model used in this study,

(ii) Additionally, the values of the latency and characteristic times proposed in section 4.4 of this report to be should be used and validated in subsequent numerical analytical studies of the hydropower plant when using Saouma's (2014) proposed ASR constitutive model,

(iii) A study to identify the relationship of crack growth to the ASR extent to be undertaken,

(iv) Further research be undertaken to estimate the degradation of the young's modulus and/or other critical engineering properties, as a function of the reaction extent for the hydropower plant in this study, to aid predicting the remaining life of the structure.

6 BIBLIOGRAPHY

Achenbach, J.D. 2009. Structural health monitoring – What is the prescription? *Mechanics Research Communications*. 36(2): 137-142.

Ahmed, T. Burley, E. Rigden, S. & Abu-Tair, A.I. 2003. The effect of Alkali Reactivity on the Mechanical Properties of concrete. *Construction and Building Materials*. 17:123-144.

Arcangeli, E. & Stella, C. 1993. The use of prestressed anchors at the Owen Falls refurbishment. *Water Power & Dam Construction*. 45:23-30.

Bangert, F. Kuhl, D. & Meschke, G. 2004. Chemo-hygro-mechanical modelling and numerical simulation of concrete deterioration caused by alkali-silica reaction. *International Journal for Numerical and Analytical Methods in Geomechanics.* 28(7-8):689-714.

Bazant, Z.P. 1994. Recent Advances in Fracture Mechanics, Size effect and Rate Dependence of Concrete: Implications for Dams. *Proceedings of the International Workshop on Dam Fracture and Damage. Chambery, France.* 41-54.

Bazant, Z.P. & Meyer, C. 2000. Fracture Mechanics of ASR in Concretes with Waste Glass Particles of Different Sizes. *Journal of Engineering Mechanics*. 226-232.

Bazant, Z.P. & Steffens, A. 2000. Mathematical Model for Kinetics of Alkali-Silica Reaction in Concrete. *Cement and Concrete Research*. 30:419-428.

Bertlin, P.D. & Olivier, H. 1954. Owen Falls: Constructional Problems. *Proceedings of the Institution of Civil Engineers*. 3(6):670-701.

Biot, M. 1955. Theory of elasticity and consolidation for a porous anisotropic solid. *Journal of Applied Physics.* 26(2):182-185.

Blight, G.E. & Alexander, M.G. 2011. Alkali-Aggregate Reaction and Structural Damage to Concrete: Engineering Assessment, Repair and Management. *Taylor & Francis Group*.1-241.

Capra, B. & Bournazel, J. -P. 1998. Modeling of induced mechanical effects of alkali-aggregate reactions. *Cement and Concrete Research.* 28(2):251-260.

Capra, B. & Sellier, A. 2003. Orthotropic modelling of alkali-aggregate reaction in concrete structures: numerical simulations. *Mechanics of materials.* 35(8):817-830.

Clark, L.A. 1989. A Critical Review of the Structural Implications of the Alkali Silica Reaction in Concrete. Contractor Report 169. *Transport and Road Research Laboratory. Crowthorne*. 1-96.

Comby-Peyrot, I. Bernard, F. Bouchard, P.-O. Bay, F. & Garcia-Diaz, E. 2009. Development and validation of a 3d computational tool to describe concrete behaviour at mesoscale: application to the alkali-silica reaction. *Computational Materials Science.* 46(4):1163-1177.

Comi, C. Fedele, R. & Perego, U. 2009. A Chemo-Thermo-Damage Model for the Analysis of Concrete Dams Affected by Alkali-Silica Reaction. *Mechanics of Materials*. 41:210-230.

Dassault Systems Simulia Corp. 2014. *Abaqus/CAE Theory Manual*. Providence: Dassault Systems.

Dassault Systems Simulia Corp. 2014. *Abaqus/CAE User's Manual*. Providence: Dassault Systems.

Dent Glasser, L.S. & Kataoka, N. 1981. The Chemistry of 'Alkali-Aggregate' Reaction. *Cement and Concrete Research*. 11:1-9.

Dolen, T.P. 2005. Materials Properties Model of Aging Concrete. *Water Resources Research Laboratory. Denver, Colorado*. 1-51.

Dolen, T.P. Scott, G.A. von Fay, K.F. & Hamilton, B. 2003. Effects of Concrete Deterioration on Safety of Dams. *U.S. Department of the Interior Bureau of Reclamation*. DSO-03-05:1-65.

Dunant, C. & Scrivener, K. 2010. Micro-mechanical modelling of alkali-silica-reaction-induced degradation using the amie framework. *Cement and Concrete Research.* 40(4):517-525.

Esposito, R. 2016. The Deteriorating Impact of Alkali-Silica Reaction on Concrete: Expansion and Mechanical Properties. *Universiteit Parma, Italie*. 1-211.

Fan, S. & Hanson, J.M. 1998. Effect of Alkali Silica Reaction Expansion and Cracking on Structural Behaviour of Reinforced Concrete Beams. *ACI Structural Journal*. 498-505.

Folliard, K.J. Thomas, M.D.A. Fournier, B. Kurtis, K.E. & Ideker, J.H. 2006. Interim Recommendations for the Use of Lithium to Mitigate or Prevent Alkali-Silica Reaction (ASR). *U.S. Department of Transportation, Federal Highway Administration.* 1-95.

Fournier, B. & Berube, M.-A. 2000. Alkali-Aggregate Reaction in Concrete: A Review of Basic Concepts and Engineering Implications. *Canadian Journal of Civil Engineering*. 27:167-191.

Fournier, B. Berube, M.-A. Folliard, K.J. & Thomas, M. 2010. Report on the Diagnosis, Prognosis, and Mitigation of Alkali-Silica Reaction (ASR) in Transportation Structures. *U.S. Department of Transportation, Federal Highway Administration*.1-154.

Gautam, B.P. 2016. Multiaxially Loaded Concrete Undergoing Alkali-Silica Reaction (ASR). *University of Toronto*. 1-196.

Ghasemi, Y. 2017. Aggregates in Concrete Mix Design. *Lulea University of Technology*. 1-118.

Giaccio, G. Zerbino, R. Ponce, J.M. & Batic, O.R. 2008. Mechanical Behaviour of Concretes Damaged by Alkali-Silica Reaction. *Cement and Concrete Research*. 38:993-1004.

Giorla, A.B. 2013. Modelling of Alkali-Silica Reaction under Multi-Axial Load. *Ecole Polytechnique Federale De Lausanne*. 1-196.

Grimal, E. Sellier, A. Multon, S. Le Pape, Y. & Bourdarot, E. 2010. Concrete modelling for expertise of structures affected by alkali aggregate reaction. *Cement and Concrete Research.* 40(4):502-507.

Hafci, A. 2013. Effect of Alkali-Silica Reaction Expansion on Mechanical Properties of Concrete. *Middle East Technical University*. 1-116.

Hui, L. & Jinping, O. 2011. Structural Health Monitoring: From Sensing Technology Stepping to Health Diagnosis. *Procedia Engineering*. 14(0): 753-760.

Ichikawa, T. & Miura, M. 2007. Modified Model of Alkali-Silica Reaction. *Cement and Concrete Research*. 37:1291-1297.

Islam, M.S. & Akhtar, S. 2013. A Critical Assessment to the Performance of Alkali-Silica Reaction (ASR) in Concrete. *Canadian Chemical Transactions*. 1(4):253-266.

Jankowiak, T. & Lodygowski, T. 2005. Identification of Parameters of Concrete Damage Plasticity Constitutive Model. *Foundations of Civil and Environmental Engineering*. 6:53-69.

Johnson, D.K. Wamock, R.L. Schindler, A.K. & Barnes, R.W. 2014. Effectiveness of Silane in Mitigating Alkali-Silica Reaction in the BIBB Graves Bridge. *Alabama Department of Transportation*. 1-230.

Jones, A.E.K. & Clark, L.A. 1998. The effects of ASR on the properties of Concrete and the Implications for Assessment. *Engineering Structures*. 20(9):785-791.

Jurcut, A.-C. 2015. Modelling of Alkali-Aggregate Reaction effects in Reinforced Concrete Structures. *University of Toronto*. 1-136.

Kmiecik, P. & Kaminski, M. 2011. Modelling of Reinforced Concrete Structures and Composite Structures with Concrete Strength Degradation taken into consideration. *Archives of Civil and Mechanical Engineering*. XI(3):623-636.

Lubliner, J. Oliver, J. Oller, S. & Onate, E. 1989. A Plastic-Damage Model for Concrete. *Int. J. Solids Structures*. 25(3):299-326.

Makha, R. & Moyo, P. 2012. Finite Element Analysis Calibration of Arch Dams Models Using Ambient Vibration Properties. *University of Cape Town*. 1-96.

Mapulanga, E.P. & Moyo, P. 2015. Modelling Concrete Swelling due to Alkali-Silica Reactions. *University of Cape Town*. 1-77.

Marzouk, H. & Langdon, S. 2003. The effect of Alkali-Aggregate Reactivity on the Mechanical properties of high and normal Strength Concrete. *Cement & Concrete Composites*. 25:549-556.

Mason, P.J. & Molyneux, J.D. 1998. The Effect of Concrete Expansion at Owen Falls Power Station, Uganda. *Proceedings of the Institution of Civil Engineers – Water Maritime and Energy*. 130(4):226-237.

McDonald, J.E. & Curtis, N.F. 1999. Repair and Rehabilitation of Dams: Case Studies. *U.S. Army Corps of Engineers: Engineer Research and Development Center*.1-263.

McLeish, A. 1990. Structural Implications of the Alkali Silica Reaction in Concrete. Contractor Report 177. *Transport and Road Research Laboratory. Crowthorne*. 1-110.

Medeiros, M. & Helene, P. 2008. Efficacy of Surface Hydrophobic Agents in Reducing Water and Chloride Ion Penetration in Concrete. *Materials and Structures*. 41:59-71.

Multon, S. Seignol, J.-F. & Toutlemonde, F. 2005. Structural Behaviour of Concrete Beams Affected by Alkali-Silica Reaction. *ACI Materials Journal*.67-76.

Multon, S. & Toutlemonde F. 2006. Effect of Applied Stresses on Alkali-Silica Reaction-Induced Expansions. *Cement and Concrete Research*. 36:912-920.

Mundeli, S. & Moyo, P. 2014. Behaviour of RC Beams Patch Repaired and Strengthened with FRP Composites: A Numerical Study. *University of Cape Town*. 1-145.

Nzuza, M.H.S. & Moyo, P. 2013. Thermo-Mechanical Modelling of Arch Dams for Performance Assessment. *University of Cape Town*. 1-136.

Pan, J.W. Feng, Y.T. Wang, J.T. Sun, Q.C. Zhang, C.H. & Owen, D.R.J. 2012. Modelling of alkali-silica reaction in concrete: a review. *Front. Struct. Civ. Eng*. 6(1):1-18.

Puatatsananon, W. & Saouma, V. 2013. Chermo-Mechanical Micromodel for Alkali-Silica Reaction. *ACI Materials Journal*. 67-77.

Republic of South Africa. 1998. *Government Gazette: National Water Act*. 398(19182):1-101.

Rodriguez, J. Gonzalez, P. Martinez, F. & Marti, J. 2011. Concrete Swelling in Existing Dams. *SIMULIA Customer Conference*. 1-15.

Saouma, V.E. 2014. Numerical Modelling of AAR. *Taylor & Francis Group*.1-317.

Saouma, V. & Perotti, L. 2006. Constitutive Model for Alkali-Aggregate Reactions. *ACI Materials Journal*. 194-202.

Saouma, V. Perotti, L. & Shimpo, T. 2007. Stress Analysis of Concrete Structures Subjected to Alkali-Aggregate Reactions. *ACI Structural Journal*. 532-541.

Schlangen, E. & Copuroglu, O. 2007. Concrete damage due to asr: a new method to determine the properties of the expansive gel. *Proceedings Framcos6.* 17-22.

Sellier, A. Grimal, E. Multon, S. & Bourdarot, E. (Editors) 2017. Swelling Concrete in Dams and Hydraulic Structures. *ISTE Ltd and John Wiley & Sons, Inc*. 1-251.

Sumer, Y. & Aktas, M. 2015. Defining Parameters for |Concrete Damage Plasticity Model. *Challenge Journal of Structural Mechanics*. 1(3):149-155.

Thomas, M.D.A. Folliard, K.J. Fournier, B. Rivard, P. & Drimalas, T. 2013. Methods for Evaluating and Treating ASR-Affected Structures: Results of Field Application and Demonstration Projects – Volume I: Summary of Findings and Recommendations. *U.S. Department of Transportation, Federal Highway Administration*. 1-80.

Thomas, M.D.A Fournier, B. & Folliard, K.J. 2012. Selecting Measures to Prevent Deleterious Alkali-Silica Reaction in Concrete: Rationale for the AASHTO PP55 Prescriptive Approach. *U.S. Department of Transportation, Federal Highway Administration.* 1-58.

Thomas, M. Fournier, B. Folliard, K. Ideker, J. & Shehata, M. 2006. Test Methods for Evaluating Preventive Measures for Controlling Expansion due to Alkali-Silica Reaction in Concrete. *Aggregates Foundation for Technology, Research and Education*. ICAR 302-1:1-62.

Trucano, T.G. Swiler, L.P. Igusa, T. Oberkampf, W.L. & Pilch, M. 2006. Calibration, validation, and sensitivity analysis: What's what. *Reliability Engineering & System Safety*. 91(0): 1331-1357.

Ulm, F.-J. Coussy, O. Kefei, L. & Larive, C. 2000. Thermo-Chemo-Mechanics of ASR Expansion in Concrete Structures. *Journal of Engineering Mechanics*. 233-242.

U.S. Department of Transportation. 2012. Alkali-Aggregate Reactivity (AAR) Workshops for Engineers and Practitioners. *U.S. Department of Transportation, Federal Highway Administration*. 1-108.

Vezi, M. & Moyo, P. 2014. Dynamic Modelling of Arch Dams in the Ambient State. *University of Cape Town*. 1-131.

Westlake, C.R. Mountain, R.W. & Paton, T.A.L. 1954. Owen Falls, Uganda, Hydro-Electric Development. *Proceedings of the IEE – Part I: General*. 101(132):347-362.

West, G. 1996. Alkali-Aggregate Reaction in Concrete Roads and Bridges. *Thomas Telford Publications*.

Xing Wen, H. 1993. Prediction of Structural Effects in Concrete affected by Alkali-Aggregate Reaction. *University of Plymouth*. 1-268.

Zappitelli, M.P. Villa, E.I. Fernandez-Saez, J. & Rocco, C. 2014. Cracking Development Prediction in Concrete Gravity Dams using *Concrete Damage Plasticity Model*. *Mecanica Computacional*. XXXIII:909-921.

APPENDIX: Example input file used for the Numerical Modelling

```
*Heading
** Job name: 10_units_Rev3 Model name: 10_units_Rev3
** Generated by: Abaqus/CAE 6.14-1
*Preprint, echo=NO, model=NO, history=NO, contact=NO
**
** PARTS
**
*Part, name=P10_units-2
*Node
      1,          10.29,    18.5400009,   -7.03999996
      2,          10.29,    18.5400009,    162.729996
      3,          10.29,    19.1499996,    162.729996
      4,          10.29,    19.1499996,   -7.03999996
      5,    18.2299995,    18.5400009,    162.729996
      6,    18.2299995,    19.1499996,    162.729996
      7,    18.2299995,    19.1499996,   -7.03999996
      8,    18.2299995,    18.5400009,   -7.03999996
      9,    18.2299995,    18.5400009,   -6.63000011
     10,    16.5499992,    18.5400009,   -6.63000011
                              :
                              :
115506,    2.74060345,    16.8199997,    37.5068665
 115507,    3.61910534,    16.8199997,    30.3363762
 115508,    4.17999983,    17.9850006,    70.3399963
 115509,     3.9968667,    16.8199997,     30.109396
 115510,   -6.44581509,    9.46500015,    68.1900024
 115511,   -6.88290787,    9.46500015,    68.1900024
 115512,    -7.9232235,    11.0244322,    72.2272034
*Element, type=C3D10, ELSET=Elemento
   1,    155,   8737,    342,    156, 17714, 17713, 17712, 17716, 17715, 17717
   2,    341,   8503,   8737,   8736, 17720, 17719, 17718, 17722, 17721, 17723
   3,    349,   8500,   8813,    149, 17726, 17725, 17724, 17728, 17727, 17729
   4,    347,   8499,   8744,   8806, 17732, 17731, 17730, 17734, 17733, 17735
   5,   8437,   8187,   4806,   8423, 17738, 17737, 17736, 17740, 17739, 17741
```

```
6,   193,   305,  8749,  8517, 17744, 17743, 17742, 17746, 17745, 17747
   7,   142,  8496,   141,  8740, 17750, 17749, 17748, 17752, 17751, 17753
   8,  8522,   293,   204,   205, 17756, 17755, 17754, 17758, 17757, 17759
   9,   209,  8524,  8525,  8818, 17762, 17761, 17760, 17764, 17763, 17765
  10,  4806,  8423,    35,  8437, 17741, 17767, 17766, 17736, 17740, 17768
                                    :
                                    :
65327,  14238,  14018,   7811,  13699, 115334, 100172,  97013, 100094,
103790,  81835
65328,  12305,   7501,   2643,   7230,  72610,  72582, 102990,  72608,
72583,  72584
65329,   3590,    943,   3420,   3588,  95920,  87828, 100098,  95960,
95959,  99575
65330,   4068,   3167,   4074,   4367, 113388,  82406, 113389, 111932,
81840, 103789
65331,  17230,   7807,   4346,  13988,  76871,  83335,  83334,  76888,
76895,  83348
65332,  12314,   2598,   3292,   7184, 107558,  75973,  81630,  81632,
109840,  81631
65333,   7280,   7500,   7501,   7282,  76857,  76806,  76859,  98438,
98436, 100042
** Section: Concrete
*Solid Section,elset=Elemento,material=Concrete
,
*End Part
**
**
** ASSEMBLY
**
*Assembly, name=Assembly
**
*Instance, name=P10_units-2-1, part=P10_units-2
          0.,           0.,           0.
          0.,           0.,           0.,           1.,           0.,
0.,          90.
*End Instance
**
*Nset, nset=Boundary, instance=P10_units-2-1
```

```
      1,       2,       3,       4,     373,     374,     375,     376,     416,
419,     420,     423,     424,     427,     428,     431
    432,     435,     436,     439,     440,     443,     444,     447,     554,
555,     562,     563,     566,     567,     570,     573
    578,     579,     582,     583,     586,     589,     594,     595,     598,
599,     602,     605,     610,     611,     614,     615
    618,     621,     626,     627,     630,     631,     634,     637,     642,
643,     646,     647,     650,     653,     658,     659
    662,     663,     666,     669,     674,     675,     678,     681,     682,
684,     686,     688,     690,     692,     694,     696
                                        :
                                        :
109752, 109963, 110105, 110163, 110525, 110526, 110531, 110549, 110570,
110660, 110661, 111202, 111879, 111905, 111950, 111951
 112180, 112210, 112573, 112624, 112739, 112754, 112783, 112792, 112846,
112965, 112970, 113009, 113027, 113059, 113073, 113074
 113118, 113340, 113536, 113695, 114045, 114396, 114397, 114406, 114448,
114516, 114542, 114819, 115071, 115129
*Elset, elset=Boundary, instance=P10_units-2-1
7622,  7628,  7630,  7680,  7681,  7758,  7761,  7787,  7826,  7829,  7832,
7836,  7838,  7844,  7845,  7846
  7847,  7924,  7939,  7946,  7947,  7950,  7956,  7976,  7985,  7988,
7989,  7999,  8002,  8049,  8084,  8120
  8138,  8140,  8147,  8149,  8165,  8176,  8202,  8234,  8246,  8247,
8272,  8276,  8296,  8297,  8299,  8301
                                      :
                                      :
63149, 63207, 63413, 63433, 63459, 63504, 63508, 63579, 63734, 63736,
63771, 63865, 63967, 63982, 64129, 64134
 64174, 64184, 64185, 64443, 64512, 64544, 64640, 64671, 64709, 64750,
64767, 64806, 64807, 64835, 64858, 64999
 65083, 65098, 65111, 65127, 65130, 65142, 65148, 65187, 65257
*Surface, type=ELEMENT, name="Generator loads"
"_Generator loads_S4", S4
"_Generator loads_S3", S3
"_Generator loads_S2", S2
"_Generator loads_S1", S1
*Elset, elset=_Surf-2_S3, internal, instance=P10_units-2-1
```

```
 17595, 17612, 17782, 18114, 19050, 19484, 19527, 19609, 19665, 19689,
19766, 19785, 19846, 19873, 19875, 19897
 19899, 19915, 19917, 19950, 19957, 20012, 20061, 20065, 20107, 20121,
20146, 20147, 20187, 20235, 20294, 20355
 20389, 21144, 21148, 21210, 21230, 21281, 21331, 21460, 21537, 21625,
21743, 21797, 21852, 21923, 21935, 22102
 22147, 22182, 22322, 22545, 22630, 22640, 22902, 22908, 23204, 23232,
23246, 23339, 23500, 23568, 23636, 23686
 23766, 23800, 23865, 24043, 24064, 24078, 24083, 24257, 24320, 24414,
24434, 24723, 24737, 24757, 24764, 24793
 24858, 24925, 25035, 25125, 25137, 25276, 25287, 25485, 25495, 25501,
25589, 25683, 25744, 25991, 26025, 26073
                                        :
                                        :
30980, 31018, 31033, 31040
 31074, 31224, 31243, 31277, 31284, 31761, 31853, 31868, 31873, 31890,
31939, 31949, 31978, 32036, 32094, 32362
 32489, 32558, 32611, 32653, 32742, 32747, 32891, 32916, 32997, 33015,
33303, 33420, 33425, 33514, 33899, 34164
 34282, 34685, 34707, 34933
*Surface, type=ELEMENT, name=Surf-2
_Surf-2_S3, S3
_Surf-2_S4, S4
_Surf-2_S2, S2
_Surf-2_S1, S1
*End Assembly
** ----------------------------------------------------------------
**
** MATERIALS
**
*MATERIAL, NAME=Concrete
*Density
2400
*Elastic
35E9, 0.2
*CONCRETE DAMAGED PLASTICITY
30, 0.1, 1.16, 0.67, 0.01
*CONCRETE COMPRESSION HARDENING
1.92e+07,        0.
```

```
2.962e+07,  0.0004
3.845e+07,  0.0008
4.463e+07,  0.0012
4.773e+07,  0.0016
4.724e+07,  0.0020
4.250e+07,  0.0024
3.270e+07,  0.0028
1.681e+07,  0.0032
* CONCRETE TENSION STIFFENING, TYPE=STRAIN
3.5e+06, 0.
3.11e+06, 0.000111
2.72e+06, 0.000222
2.33e+06, 0.000333
1.95e+06, 0.000444
1.56e+06, 0.000555
1.17e+06, 0.000667
0.78e+06, 0.000778
0.39e+06, 0.000889
0., 0.001
*CONCRETE TENSION DAMAGE, TYPE=STRAIN
0.,       0.
0.111, 0.000111
0.223, 0.000222
0.334, 0.000333
0.443, 0.000444
0.554, 0.000555
0.666, 0.000666
0.777, 0.000778
0.889, 0.000889
*DEPVAR
1,
*USER DEFINED FIELD
*EXPANSION, USER
**
** BOUNDARY CONDITIONS
**
** Name: boundary_1 Type: Symmetry/Antisymmetry/Encastre
*BOUNDARY
Boundary, ENCASTRE
```

```
*BOUNDARY
Boundary_2, ENCASTRE
*INITIAL CONDITIONS,TYPE=TEMPERATURE
Nodos, 15.
*INITIAL CONDITIONS,TYPE=FIELD, VARIABLE=1
Nodos, 0.
*INITIAL CONDITIONS,TYPE=FIELD, VARIABLE=2
Nodos, 0.
** STEP Loading
**
*STEP, name=Loading, INC=10000000
*STATIC
30 , 3650., 1E-35, 30
**
** LOADS
**
** Name: Hydrostatic_1   Type: Pressure
*Dsload
Surf-2, HP, 246800., 33.33, 8.65
** Name: Load-1   Type: Pressure
*Dsload
"Generator loads", P, 54205.7
**
** OUTPUT REQUESTS
**
*Restart, write, frequency=0
**
** FIELD OUTPUT: F-Output-1
**
*Output, field, number interval=90, time marks=NO
*Node Output
U,
*Element Output, directions=YES
E, S, DAMAGET, PEEQ, PE
**Output, history, number interval=90, time marks=NO
**ELEMENT OUTPUT, ELSET=Elemento
**SDV1, THE11
*End Step
```